Opportunity Mars Rover mission: Overview and selected results from Purgatory ripple to traverses to Endeavour crater

R. E. Arvidson,[1] J. W. Ashley,[2] J. F. Bell III,[3] M. Chojnacki,[4] J. Cohen,[5] T. E. Economou,[6] W. H. Farrand,[7] R. Fergason,[8] I. Fleischer,[9] P. Geissler,[8] R. Gellert,[10] M. P. Golombek,[11] J. P. Grotzinger,[12] E. A. Guinness,[1] R. M. Haberle,[13] K. E. Herkenhoff,[8] J. A. Herman,[11] K. D. Iagnemma,[14] B. L. Jolliff,[1] J. R. Johnson,[8] G. Klingelhöfer,[9] A. H. Knoll,[15] A. T. Knudson,[16] R. Li,[17] S. M. McLennan,[18] D. W. Mittlefehldt,[19] R. V. Morris,[19] T. J. Parker,[11] M. S. Rice,[3] C. Schröder,[20,21] L. A. Soderblom,[8] S. W. Squyres,[3] R. J. Sullivan,[3] and M. J. Wolff[7]

Received 24 September 2010; accepted 9 November 2010; published 8 February 2011.

[1] Opportunity has been traversing the Meridiani plains since 25 January 2004 (sol 1), acquiring numerous observations of the atmosphere, soils, and rocks. This paper provides an overview of key discoveries between sols 511 and 2300, complementing earlier papers covering results from the initial phases of the mission. Key new results include (1) atmospheric argon measurements that demonstrate the importance of atmospheric transport to and from the winter carbon dioxide polar ice caps; (2) observations showing that aeolian ripples covering the plains were generated by easterly winds during an epoch with enhanced Hadley cell circulation; (3) the discovery and characterization of cobbles and boulders that include iron and stony-iron meteorites and Martian impact ejecta; (4) measurements of wall rock strata within Erebus and Victoria craters that provide compelling evidence of formation by aeolian sand deposition, with local reworking within ephemeral lakes; (5) determination that the stratigraphy exposed in the walls of Victoria and Endurance craters show an enrichment of chlorine and depletion of magnesium and sulfur with increasing depth. This result implies that regional-scale aqueous alteration took place before formation of these craters. Most recently, Opportunity has been traversing toward the ancient Endeavour crater. Orbital data show that clay minerals are exposed on its rim. Hydrated sulfate minerals are exposed in plains rocks adjacent to the rim, unlike the surfaces of plains outcrops observed thus far by Opportunity. With continued mechanical health, Opportunity will reach terrains on and around Endeavour's rim that will be markedly different from anything examined to date.

Citation: Arvidson, R. E., et al. (2011), Opportunity Mars Rover mission: Overview and selected results from Purgatory ripple to traverses to Endeavour crater, *J. Geophys. Res.*, *116*, E00F15, doi:10.1029/2010JE003746.

[1]Department of Earth and Planetary Sciences, Washington University, St. Louis, Missouri, USA.
[2]School of Earth and Space Exploration, Mars Space Flight Facility, Arizona State University, Tempe, Arizona, USA.
[3]Department of Astronomy, Cornell University, Ithaca, New York, USA.
[4]Planetary Geosciences Institute, Department of Earth and Planetary Sciences, University of Tennessee, Knoxville, Tennessee, USA.
[5]Honeybee Robotics Spacecraft Mechanisms Corporation, New York, New York, USA.
[6]Laboratory for Astrophysics and Space Research, Enrico Fermi Institute, University of Chicago, Chicago, Illinois, USA.
[7]Space Science Institute, Boulder, Colorado, USA.
[8]U.S. Geological Survey, Flagstaff, Arizona, USA.
[9]Institut für Anorganische und Analytische Chemie, Johannes Gutenberg-Universität, Mainz, Germany.
[10]Department of Physics, University of Guelph, Guelph, Ontario, Canada.
[11]Jet Propulsion Laboratory, California Institute of Technology, Pasadena, California, USA.
[12]Division of Geological and Planetary Sciences, California Institute of Technology, Pasadena, California, USA.
[13]NASA Ames Research Center, Moffett Field, California, USA.
[14]Department of Mechanical Engineering, Massachusetts Institute of Technology, Cambridge, Massachusetts, USA.
[15]Department of Organismic and Evolutionary Biology, Harvard University, Cambridge, Massachusetts, USA.
[16]Planetary Science Institute, Tucson, Arizona, USA.
[17]Department of Civil and Environmental Engineering and Geodetic Science, Ohio State University, Columbus, Ohio, USA.
[18]Department of Geosciences, State University of New York at Stony Brook, Stony Brook, New York, USA.
[19]NASA Johnson Space Center, Houston, Texas, USA.
[20]Department of Hydrology, University of Bayreuth, Bayreuth, Germany.
[21]Center for Applied Geoscience, Eberhard Karls University of Tübingen, Tübingen, Germany.

0148-0227/11/2010JE003746

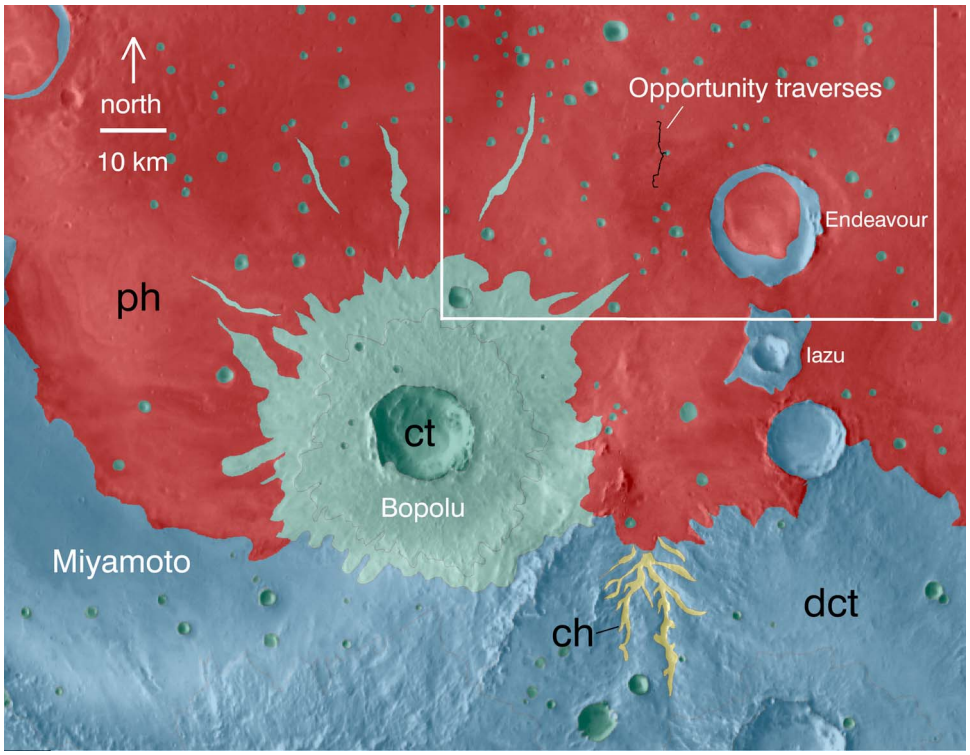

Figure 1. Geologic map for the southern portion of the Meridiani Planum layered sedimentary rocks (ph, hematite-bearing plains) and the Noachian-aged dissected cratered terrain (dct). Miyamoto is a partially buried impact basin that predates deposition of the layered sedimentary sequence. Endeavour and Iazu are Noachian craters partially buried by the layered materials, as is the channel system mapped as "ch." The ph unit unconformably overlies the dct and ch units and is interpreted from impact crater densities to have been emplaced in late Noachian to early Hesperian times [*Arvidson et al.*, 2006]. The impact event that produced the crater Bopolu penetrated below the layered materials (ph) and into the underlying Noachian cratered terrain materials (dct). These older materials are exposed on the crater floor and ejecta deposits. Opportunity's ~22 km (as of 27 July 2010) of traverses are overlain as a black line. A THEMIS daytime IR mosaic was used as a map base. White box delineates area shown in Figure 11.

1. Introduction

[2] The Mars Exploration Rover (MER) Opportunity touched down on the Meridiani plains on 25 January 2004 (Figures 1–2). Since landing, Opportunity has conducted numerous traverses and made extensive measurements with its Athena science payload (Table 1), including examination of impact crater ejecta deposits, rims, and walls to access and characterize stratigraphic rock sections within the Burns formation [e.g., *Squyres and Knoll*, 2005], detailed examination of a variety of cobbles and boulders exposed on the surface, and characterization of the aeolian ripples that partially cover plains outcrops. In addition, numerous atmospheric opacity and cloud measurements have been acquired using Pancam and Navcam, and the Alpha Particle X-Ray Spectrometer (APXS) has been used to monitor atmospheric argon mixing ratios.

[3] The purpose of this paper is to summarize operations and present selected scientific highlights from the time Opportunity left the Purgatory (unless otherwise noted, names for features used in this paper are informal) aeolian ripple on sol 511 (1 July 2005) to the first relatively high spatial resolution views of the Endeavour crater rim on sol 2300 (13 July 2010; Figure 1 and Table 2). The paper also includes a synthesis of orbital and rover-based data for areas along and close to Opportunity's traverses for interpretations of material properties, morphology, and geologic histories on both local and regional scales. This overview is meant to complement papers that provide detailed findings from Opportunity's measurements that are included as the fourth set of Mars Exploration Rover papers published in the Journal of Geophysical Research and also published elsewhere over the past several years. For reference, *Squyres et al.* [2003] provide a summary of the Athena science payload and *Squyres et al.* [2006] summarize Opportunity mission results up to embedding into and extrication from the Purgatory ripple, i.e., up to sol 510.

2. Background Discussion

[4] MER Mission science objectives are focused on remote sensing and in situ observations along traverses to characterize current and past Martian environments and the role of water in formation and alteration of the surface and associated crustal materials [*Squyres et al.*, 2003]. These objectives are aligned with the overarching NASA Mars Exploration Program themes of "follow the water" and searching for evidence of past or present habitable zones and

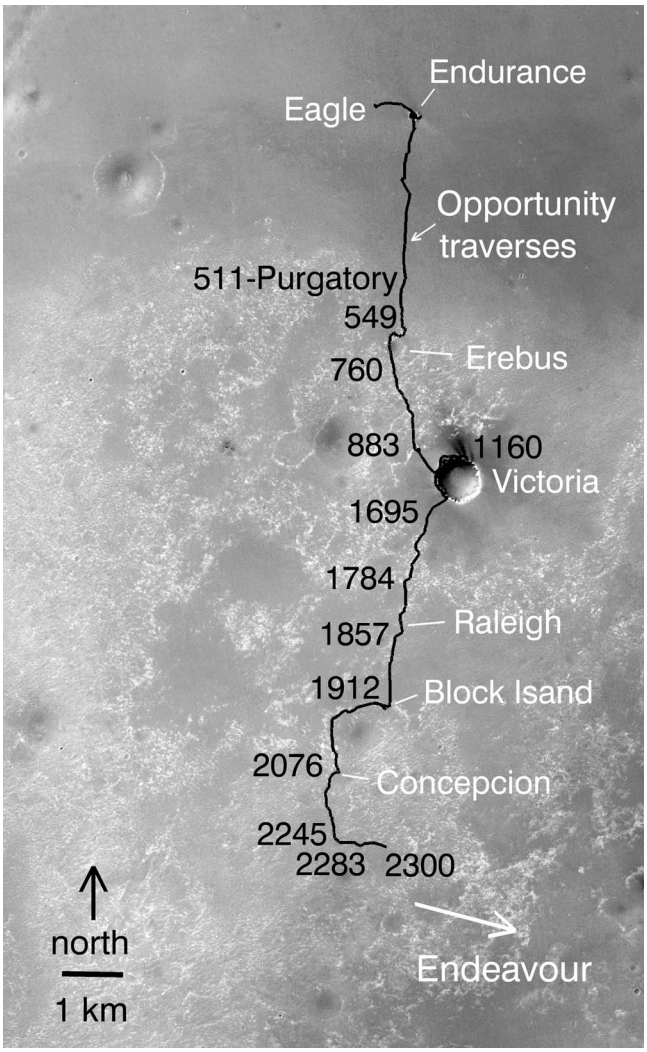

Figure 2. Portion of a CTX image P15_006847_1770_XN_03S005W_080111 covering Opportunity's traverses and immediate surroundings. Eagle, Endurance, Erebus, Victoria, Raleigh, and Concepción craters are shown, along with the traverse direction to Endeavour, located about 11 km to the southeast of the sol 2300 location. Block Island is an iron meteorite discovered south of Victoria. Key sols are shown, including the location of the Purgatory ripple, where the previous overview paper [*Squyres et al.*, 2006] ended its summary of operations and science highlights. Bright areas correspond to regions with extensive outcrop, whereas darker areas are widely covered by aeolian ripples.

life. For reference, on the other side of the planet the Spirit rover has been exploring the Inner Basin, Columbia Hills, Gusev crater, and has acquired data that indicate the presence of hydrated sulfate, opaline, and carbonate-bearing mineral deposits of likely fumarolic or hydrothermal origins [*Arvidson et al.*, 2008, 2010; *Squyres et al.*, 2008; *Morris et al.*, 2010]. Opportunity landed on the Meridiani plains, selected primarily because the Mars Global Surveyor Thermal Emission Spectrometer (TES) data indicated a high abundance of hematite, a mineral typically formed in an aqueous environment [*Christensen et al.*, 2001]. Data collected by Opportunity within Eagle and Endurance craters conclusively showed that the hematite signature is carried by hematitic concretions weathered from sulfate-rich bedrock and concentrated as a surface lag, partly worked into basaltic sand ripples that cover much of the plains [*Soderblom et al.*, 2004; *Sullivan et al.*, 2005; *Arvidson et al.*, 2006; *Jerolmack et al.*, 2006]. Further, the sulfate-rich sandstones that comprise the Burns formation and that underlie the ripples were found to be largely ancient aeolian sandstone deposits, with local reworking within ephemeral lakes [*Squyres et al.*, 2004; *Grotzinger et al.*, 2005, 2006; *Metz et al.*, 2009]. Post depositional aqueous processes have altered the deposits as evidenced by the presence of hematitic concretions and fracture-filling deposits [*McLennan et al.*, 2005; *Knoll et al.*, 2008]. Opportunity has continued to search for the mud-rich rock facies that would help confirm the hypothesis that the sands formed from precursor evaporates in a playa lake environment.

[5] The Burns formation rocks examined by Opportunity are part of a regional-scale deposit that covers several hundred thousand square kilometers and is best explained by accumulation during one or more periods of rising groundwater [e.g., *Andrews-Hanna et al.*, 2010] (Figure 1). These deposits are draped unconformably onto dissected cratered terrain and exhibit an impact crater size frequency distribution indicative of a preservation age of Noachian or Early Hesperian [*Arvidson et al.*, 2006]. Preexisting craters are also evident and show partial burial by the sedimentary deposits, including the ~20 km diameter Endeavour crater toward which Opportunity is traversing (Figure 1). Bopolu is a ~19 km diameter crater located to the southwest of Opportunity (Figure 1). This crater clearly postdates the deposition of the sulfate-rich sedimentary deposits, given that the floor and rim of the crater, along with its ejecta deposits, exhibit basaltic signatures [*Christensen et al.*, 2001] and the ejecta deposits extend over the sedimentary deposits (Figure 1). Bopolu, and other rayed craters on Meridiani Planum, lack hematite signatures on their ejecta deposits, implying that these craters formed after the hematite was concentrated on the surface [*Golombek et al.*, 2010]

[6] Detailed measurements conducted by Opportunity in Eagle and Endurance craters showed the utility of impact craters for assessing the stratigraphy of the layered sedimentary rocks within Merdiani Planum [e.g., *Squyres et al.*, 2006]. This approach was continued during the period of the mission covered by this paper, including measurements of strata within Erebus and Victoria craters, together with remote sensing and in situ observations of smaller craters and ejecta deposits encountered during traverses. Opportunity has also continued to characterize aeolian deposits, cobbles, and the atmosphere. Key results for all of these measurements are presented in this paper, along with brief summaries of instrument and vehicle status, and a chronicle of traverses and measurements from sols 511 to 2300.

3. Mission Overview

3.1. Rover and Payload Status

[7] From sol 1 to sol 2300 Opportunity traversed 21,760 m and from sol 511 to sol 2300 16,389 m were covered, based on tracking wheel turns (Figure 2). For reference, Table 1

Table 1. Opportunity's Payload Elements[a]

Instrument	Key Parameters
Mast-Mounted Science Instruments	
Pancam: Panoramic Camera	Multispectral imager (~400 to 1000 nm) with stereoscopic capability; 0.28 mrad IFOV; 16.8 deg by 16.8°FOV. Stereo baseline separation of 30 cm. External calibration target on rover deck.
Mini-TES: Thermal Emission Spectrometer	Emission spectra (5 to 29 μm, 10 cm^{-1} resolution) with 8 or 20 mrad FOV. Internal and external blackbody calibration targets. Instrument put in "stand down" mode on sol 2257 after failing to respond to commands.
Instrument Deployment Device (IDD)-Mounted In Situ Package	
APXS: Alpha Particle X-Ray Spectrometer	^{244}Cm alpha particle sources, and x-ray detectors, 3.8 cm FOV.
MB: Mössbauer Spectrometer	^{57}Fe spectrometer in backscatter mode; ^{57}Co/Rh source and Si-PIN diode detectors; field of view approximately 1.5 cm.
MI: Microscopic Imager	31 μm/pixel monochromatic imager (1024 × 1024) with 2 mm depth of field.
RAT: Rock Abrasion Tool	Tool capable of brushing surfaces and grinding 5 mm deep by 4.5 cm wide surface on rocks.
Engineering Cameras	
Navigation Cameras (Navcam)	Mast-mounted panchromatic stereoscopic imaging system with 0.77 mrad IFOV; 45°FOV, and 20 cm stereo baseline separation.
Hazard Avoidance Cameras (Hazcam)	Front and rear-looking panchromatic stereoscopic imaging systems with 2 mrad IFOV; 123°FOV, 10 cm stereo baseline separation.

[a]Magnets were also included on the spacecraft but not described in this table.

provides a summary of the Athena science payload, with selected comments about status. Opportunity and its Athena payload were not designed and built to travel over thousands of meters and operate over six and one half years. Even so, the vehicle and payload have continued to operate well.

[8] Opportunity's right front steering actuator failed on sol 433, leaving the wheel rotated inward by an ~8 degree angle. On sol 654 the Instrument Deployment Device (IDD) experienced an unstow anomaly because of a failing shoulder joint actuator. This joint was declared "failed" on sol 1542 and since then the IDD has been left deployed forward, carried in a "fishing stow" position while driving. IDD deployments have still been possible, but within a more limited work volume as compared to earlier measurements. Wheel currents for the right front wheel have occasionally spiked during drives, perhaps because of uneven distribution of lubricant. The solution has been to rotate the affected wheel backward and forward to even out the lubricant and to "rest" the wheel when currents spiked to particularly high values. The vehicle has primarily been driven backward during the mission period covered by this paper, in part to minimize wheel actuator current spikes, and because this mode was found to permit Opportunity to cross ripples with minimal mobility difficulties.

[9] Opportunity has survived four Martian summers, with their associated dust storms and periods of high atmospheric opacity (Figure 3). Solar array energy has varied widely from low values during the winter to high values during the summer, with strong modulations based on the amount of dust in the atmosphere and on the solar panels. Dust accumulation on the panels was predicted to end rover life much earlier, but winds have removed dust on sols 520, 1150, 1305, 1520 (minor), 1620, 1846 (minor), 1990 (minor), and 2300, providing instantaneous increases in available energy. Unlike Spirit, which is located at −14.57° latitude, Opportunity's near equatorial location (−1.95° latitude) has provided enough sunlight to allow the vehicle to continue operations throughout the winter seasons, although at a reduced pace relative to summer operations.

[10] Dust coatings on the Pancam optical surfaces have made radiometric calibration of images a continuing and involved process, particularly because the Pancam calibration target on the rover deck has also accumulated dust. Dust has accumulated on the Navcam and Hazcam exterior optical surfaces, but has not compromised the use of these cameras for either scientific purposes or operations, including driving and IDD deployment planning. During calendar year 2007 (~sol 1240, Figure 3) a global dust storm deposited dust on the Microscopic Imager (MI) exterior optics, both inside and outside the protective dust cover. The dust cover seal is not airtight as it was designed to allow gas to escape during launch. Consequently, useful MI images can no longer be acquired with the dust cover closed, and images taken with the dust cover open are visibly affected by dust contamination. This contamination has reduced the signal/noise in Opportunity MI images, but has not affected the ability to retrieve useful textural information from the data. Unfortunately, dust accumulation on the Mini-TES exterior mirror compromised the ability to retrieve quantitative information about mineralogy from data acquired after ~sol 1217. The instrument ceased responding to commands from the rover on sol 2257.

[11] The Alpha Particle X-Ray Spectrometer (APXS) has continued to operate nominally, acquiring compositional information for soils and rocks and making measurements of atmospheric argon. The Mössbauer Spectrometer (MB) has also continued to acquire data for soils and rocks, although significant decay of the cobalt-57 radioactive source (271.79 day half-life) eventually required measurements extending over several sols to achieve appropriately high spectral signal to noise values. The Rock Abrasion Tool (RAT) has ground into 38 rocks over the course of the mission. During the period covered by this paper 18 rocks were brushed and 15 were ground. By sol 2300 the grinding bit pads were worn to ~20 to 30% of their original thicknesses and the brush was slightly bent, no longer sweeping out a complete circle. All three RAT encoder motors have stopped operating, leading to step-by-step manual approaches for commanding the RAT to avoid a brush or grind failure or damage to the instrument.

3.2. Overview of Mission Activities

[12] Table 2 provides a sol-by-sol description of Opportunity's activities. Figure 3 shows a timeline of major activities with available solar panel energy and atmospheric opacity on a sol-by-sol basis. Traverses have been mainly from north to south, with stops in or near craters to examine rock strata and other "jogs" to examine important science targets or avoid large ripples (informally termed "purgatoids" after the Purgatory ripple, where Opportunity was embedded between sols 446 and 484) (Figure 2). By ~sol

Table 2. Major Activities for Opportunity Organized by Sol[a]

Earth Date[b]	Sol	Activity	Site
7/1/05–7/4/05	511–514	Leave "Purgatory" ripple; RS	55
7/5/05–7/7/05	515–517	Drive east toward "Erebus crater"; RS	55
7/8/05–7/9/05	518–519	RS; recharge batteries	56
7/10/05–7/14/05	520–524	Drive east toward "Erebus crater," first use of combined short segments of blind driving with small slip check segments; RS	56
7/16/05–8/5/05	525–545	RS; Right front steering actuator diagnostic test; Recharge; Continue drive east toward "Erebus crater"	56–57
8/6/05–8/23/05	546–562	Cobble field: IDD "OneScoop," "Arkansas" cobble, "Perseverance" cobble, "Reiner_Gamma" soil target, "Fruit_Basket" outcrop, and "Lemon_Rind" and "Strawberry" targets	58
8/24/05–9/3/05	563–573	Anomaly and recovery; RS	59
9/4/05–9/7/05	574–577	RS	58
9/8/05–9/11/05	578–581	Continue drive east toward "Erebus crater"; RS	59
9/12/05–9/13/05	582–583	Arrive "Erebus Highway," Continue drive east toward "Erebus crater"	60
9/12/05–9/21/05	584–591	Continue drive east toward "Erebus crater; RS	60
9/23/05–9/26/05	592–595	Arrive "Erebus crater"; "South Shetland" Feature: Approach and IDD "Deception" target	62
9/27/05–9/29/05	596–598	Warm Reboot Anomaly, Stand Down, and Recover	62
9/30/05–10/1/05	599–600	RS, 360 degree Panorama	62
10/2/05–10/5/05	601–604	Drive northwest around "Erebus crater"; RS	62
10/6/05	605	Backward drive out of ripple to outcrop	62
10/7/05–10/10/05	606–609	Drive westward around "Erebus crater"; RS	62
10/11/05–10/12/05	610–611	Spacecraft reset; Anomaly and recovery	–
10/13/05	612	Runout	–
10/14/05–10/31/05	613–630	Continue drive westward around "Erebus crater"; RS	62
11/2/05–11/9/05	631–638	Arrive "Olympia" outcrop: Approach and IDD "Kalavrita" and "Ziakas" targets	64
11/10/05–11/15/05	639–644	Approach, IDD, and RS "Antistasi" cobble	64
11/16/05–11/17/05	645–646	RS	64
11/18/05–11/20/05	647–649	RS; IDD Composition and Calibration Target	64
11/21/05–11/24/05	650–653	RS; Drive	64
11/25/05–11/27/05	654–656	IDD unstow failure	64
11/28/05–11/30/05	657–659	RS	64
12/1/05–12/8/05	660–667	RS; IDD diagnostics	64
12/9/05–12/11/05	668–669	RS; Atmospheric observations	64
12/12/05	670	Atmospheric RS; Coordinated photometry campaign with MEX	64
12/13/05–12/16/05	671–674	RS; Atmospheric observations, IDD successfully unstowed	64
12/17/05–12/20/05	675–678	IDD "Williams" target	64
12/21/05–12/27/05	679–685	IDD "Ted" target	64
12/28/05–1/1/06	686–690	Continue IDD "Ted" target, IDD "Hunt"	64
1/2/06–1/7/06	691–696	Continue IDD "Ted" target	64
1/8/06	697	RS	64
1/10/06–1/12/06	698–701	"Martian Tai Chi"; Atmospheric and targeted RS	64
1/13/06–1/15/06	702–704	RS; unsuccessful IDD unstow	64
1/16/06–1/18/06	705–706	Coordinated observations with MEX	64
1/19/06	707	Successful bump	64
1/20/06–1/21/06	708–709	"Olympia" Outcrop, "Lower Overgaard" feature: IDD "Scotch" target	64
1/22/06–1/23/06	710–711	Coordinated observations with MEX	64
1/24/06–1/26/06	712–714	Continue "Olympia" Outcrop, "Lower Overgaard" feature: IDD "Scotch" target	64
1/27/06–1/28/06	715–716	"Olympia" Outcrop, "Overgaard" feature: IDD "Branchwater" and "Bourbon" targets	64
1/29/06–1/30/06	717–718	RS	64
1/31/06–2/4/06	719–723	"Olympia" Outcrop, "Overgaard" feature: IDD "Don_Giovani," "Salzburg," and "Nachtmusik" targets	64
2/5/06–2/6/06	724–725	Bump to "Roosevelt"	64
2/8/06–2/12/06	726–730	"Olympia" Outcrop, "Roosevelt" feature: IDD "Rough Rider" and "Fala" targets	64
2/13/06–2/14/06	731–733	"Olympia" Outcrop, "Bellemont" feature: IDD "Vicos," "Tara," "Chaco," and "Verdun" targets	64
2/15/06–2/16/06	734–735	IDD stall; RS; short IDD diagnostic activity	64
2/17/06–2/20/06	736–739	Runout; Atmospheric Remote Science and Photometry	64
2/21/06–3/2/06	740–748	Drive toward and along "Payson" outcrop; RS	64–65
3/3/06–3/4/06	749–750	"Payson" outcrop: RS	64
3/5/06–3/12/06	751–758	Continue drive toward and along "Payson" outcrop; RS	64–65
3/13/06	759	Recharge; Atmospheric observations	65
3/14/06–3/16/06	760–762	Drive south toward "Victoria crater"; RS	65–76
3/17/06	763	Atmospheric observations	65
3/18/06–3/21/06	764–767	Continue drive south toward "Victoria crater"; RS	65–76
3/22/06–3/24/06	768–770	Odyssey safe mode; Limited downlink capability	66
3/25/06–3/26/06	771–772	Atmospheric observations; RS	66
3/27/06–3/30/06	773–776	Continue drive south toward "Victoria crater"; RS	65–76
3/31/06–4/3/06	777–779	Recharge; RS	67
4/4/06–4/14/06	780–790	Continue drive south toward "Victoria crater"; RS	65–76

Table 2. (continued)

Earth Date[b]	Sol	Activity	Site
4/15/06	791	IDD "Buffalo Springs" outcrop; RS	68
4/16/06–4/25/06	792–801	Continue drive south toward "Victoria crater"; RS	65–76
4/26/06–4/27/06	802–803	Short drive to potential IDD target outcrop	69
4/28/06–4/30/06	804–806	IDD "Brookville" target	69
5/1/06–5/9/06	807–815	Continue drive south toward "Victoria crater"; RS	65–76
5/11/06	816	Atmospheric observations	70
5/12/06	817	Continue drive south toward "Victoria crater"; RS	65–76
5/13/06–5/15/06	818–820	IDD "Cheyenne" outcrop	70
5/16/06–5/19/06	821–824	Continue drive south toward "Victoria crater"; RS	65–76
5/20/06–5/22/06	825–827	IDD "Alamogordo Creek" soil target	71
5/23/06–5/27/06	828–832	Continue drive south toward "Victoria crater"; RS	65–76
5/28/06–6/6/06	833–842	Opportunity embedded in "Jammerbugt" ripple; Extraction	71
6/7/06–6/8/06	843–844	Continue drive south toward "Victoria crater"; RS	65–76
6/9/06	845	Targeted RS	72
6/10/06–6/15/06	846–851	Continue drive south toward "Victoria crater"; RS; Atmospheric observations	72
6/16/09	852	Begin new flight software uplink	72
6/18/06–6/24/06	853–859	RS	72
6/25/06–7/7/06	860–872	Continue drive south toward "Victoria crater"; RS	65–76
7/8/06–7/13/06	873–878	Drive toward "Beagle crater"	73–74
7/14/06–7/16/06	879–881	IDD "Westport" disturbed soil target and "Fort Graham" undisturbed soil target; RS "Dallas" disturbed soil target and "Waco" outcrop	74
7/17/06–7/19/06	882–884	Runout; RS; Drive toward "Beagle Highway"	74
7/20/06–7/26/06	885–890	Approach, scuff, and IDD "Jesse Chisolm" target; IDD "Joseph McCoy" cobble, "Haiwassee" cobble	74
7/27/06	891	Approach and scuff soil target; RS	74
7/28/06	892	RS	74
7/29/06–8/1/06	893–896	IDD and RS "Baltra" outcrop pavement	74
8/2/06–8/6/06	897–901	Recharge; Drive to rim of "Beagle"; RS	74
8/7/06–8/9/06	902–904	Spacecraft fault and recovery	74
8/10/06–8/14/06	905–909	RS	74
8/15/06–8/16/06	910–911	IDD "Isabela" and "Marchena" ripple banding targets	74
8/17/06–8/23/06	912–918	Continue drive south toward "Victoria crater"; RS	65–76
8/24/06	919	IDD shoulder azimuth joint stalled; Diagnostic measurements; scuff soil	75
8/25/06–8/27/06	920–922	IDD stall	75
8/28/06–9/2/06	923–927	IDD diagnostics	75
9/3/06	928	Sol 919 scuff: IDD "Powell" and "Powell's Brother" targets	75
9/4/06	929	Drive toward "Emma Dean" crater	75
9/5/06–9/10/06	930–935	RS	75
9/11/06–9/16/06	936–941	Approach, IDD, and RS "Cape Faraday" possible ejecta target	75
9/17/06–9/22/06	942–947	Continue drive south toward "Victoria crater"; RS	65–76
9/23/06	948	Mobility tests	76
9/24/06–9/27/06	949–952	Continue drive south toward "Victoria crater"; RS	65–76
9/28/06–8/29/06	953–954	Targeted RS: "Duck Bay"	76
9/30/06–10/4/06	955–959	Drive toward "Cape Verde" promontory; RS	76
10/5/06	960	RS	76
10/6/06–10/10/06	961–964	IDD "Fogo" target	76
10/11/06–10/13/06	965–967	RS; Recharge	76
10/14/06–10/15/06	968–969	Make room in flash for conjunction data	76
10/16/06–10/30/06	970–984	Solar Conjunction; "Cape Verde" Panorama, IDD "Cha" target; Cape Verde Pan	76
10/31/06–11/6/06	985–991	Continue "Cape Verde" Panorama	76
11/7/06–11/18/06	992–1002	Drive to "Cape St. Mary" promontory; RS	76
11/19/06–11/20/06	1003–1004	Untargeted RS	76
11/21/06–11/22/06	1005–1006	MGS contact attempts; RS "Cape Verde"; Targeted RS	76
11/23/06–11/24/06	1007–1008	Targeted RS	76
11/25/06–11/28/06	1009–1012	Drive toward "Bottomless Bay"; RS	76–77
11/29/06	1013	MRO coordinated observations; RS	76
11/30/06	1014	Drive toward "Bottomless Bay"; RS	76
12/1/06	1015	RS	77
12/2/06	1016	Continue drive toward "Bottomless Bay"; RS; IDD autoplace checkout	77
12/3/06	1017	Atmospheric RS	77
12/4/06	1018	Ground survey; APXS argon density measurement	77
12/5/06–12/6/06	1019–1020	RS "Bottomless Bay"; Atmospheric RS	77
12/7/06–12/20/06	1021–1034	Drive closer to "Bottomless Bay"; RS; IDD autoplace checkout	77
12/22/06–12/23/06	1035–1036	IDD "Rio de Jeneiro" target	77
12/24/06	1037	Phoenix demo	77, 78
12/25/06	1038	Continue IDD "Rio de Jeneiro" target	77
12/26/06	1039	Drive toward "Bay of Toil"; Atmospheric RS	77–78
12/27/06	1040	APXS atmosphere	77, 78
12/28/06–1/9/07	1041–1053	Drive to, IDD, and RS "Santa Catarina" cobble	78
1/10/07	1054	Atmospheric RS	78
1/11/07–1/12/07	1055–1056	RS	78

Table 2. (continued)

Earth Date[b]	Sol	Activity	Site
1/13/07	1057	APXS argon measurement; Atmospheric RS	78
1/14/07	1058	Continue drive toward "Bay of Toil"	77, 78
1/15/07	1059	RS	78
1/16/07–1/17/07	1060–1061	"Bay of Toil" long baseline stereo RS	78
1/18/07	1062	RS cobbles, image Comet McNaught	78
1/19/07	1063	APXS argon measurement; RS	78
1/20/07–1/22/07	1064–1066	Drive toward "Cape Desire"; RS; tests to solve visual odometry "picket fence" problem	78
1/23/07–1/25/07	1067–1069	Drive toward tip of "Cape Desire"	78
1/26/07	1070	IDD and RS	78
1/27/07	1071	Continue drive toward tip of "Cape Desire"; RS	78
1/29/07	1072	RS magnets and atmosphere	78
1/30/07–1/31/07	1073–1074	Long baseline stereo RS "Cabo Corrientes"	78
2/1/07–2/3/07	1075–1077	Approach and RS "Cabo Anonimo"	78
2/4/07–2/10/07	1078–1084	Drive toward "Cabo Corrientes"; RS	79
2/11/07–2/16/07	1085–1090	Drive to position to image "Cape Desire"; Atmospheric RS	79
2/17/07–2/23/07	1091–1097	RS "Cape Desire," "ExtremaDura" outcrop and "Cape of Good Hope" ("Madrid" and "Alava" outcrops)	79
2/24/07–2/28/07	1098–1102	Drive to "Cape of Good Hope"; RS	79–80
3/1/07	1103	IDD diagnostic	79
3/2/07–3/5/07	1104–1107	Continue drive to "Cape of Good Hope"; RS	79–80
3/7/07–3/10/07	1108–1111	Drive toward "Valley Without Peril"; RS "Cape St. Vincent"	80
3/11/07	1112	RAT grind test	80
3/12/07–3/14/07	1113–1115	Continue drive toward "Valley Without Peril"; RS "Cape St. Vincent"	80
3/15/07–3/19/07	1116–1120	Race condition fault; Recover; Rest sols	–
3/20/07–3/26/07	1121–1127	Continue drive toward "Valley Without Peril"; RS "Cape St. Vincent"	80
3/27/07	1128	RAT grind diagnostics	81
3/28/07–4/1/07	1129–1133	Continue drive toward "Valley Without Peril"; RS "Cape St. Vincent"	80
4/2/07–4/4/07	1134–1136	Approach and IDD "Salamanca" and "Sevilla" soil targets (wind streaks); RS	81
4/5/07–4/6/07	1137–1138	East and west photometry	81
4/7/07–4/9/07	1139–1141	IDD and RS dark streak; RS	81
4/10/07–4/11/07	1142–1143	Drive to second location in dark streak; IDD	81
4/13/07–4/19/07	1144–1150	Drive to "Alicante" dark streak soil target, IDD, and RS; RS	81
4/20/07–4/21/07	1151–1152	Atmospheric RS	81
4/22/07–4/25/07	1153–1156	Drive to "Tierra del Fuego"; Long baseline stereo of "Cape St. Vincent"; RS	81
4/26/07	1157	Drive to "Granada"	81
4/27/07–4/28/07	1158–1159	Atmospheric RS	82
4/29/07	1160	RS; D* checkout	82
4/30/07	1161	RS "Malaga" and "Granada"	82
5/1/07–5/3/07	1162–1164	Drive toward "Cape of Good Hope"; RS	82
5/4/07	1165	Atmospheric RS	82
5/5/07–5/8/07	1166–1169	RAT touch test on "Viva La Rata"; IDD and RS	82
5/9/07	1170	IDD diagnostics; Drive to "Madrid"	82
5/10/07	1171	Drive to "Pedriza" cobble	82
5/11/07	1172	Soil thermal inertia experiment	82
5/12/07–5/13/07	1173–1174	Drive; Atmospheric RS	82
5/14/07	1175	Bump to "Cercedilla"; RS	82
5/15/07–5/23/07	1176–1183	"Cercedilla" feature: IDD "Penota" target; RS	82
5/24/07–6/13/07	1184–1204	Drive toward "Cape Verde"; RS; D* checkout, Visual Target Tracking checkout	83, 84, 85
6/14/07–6/22/07	1205–1213	Long baseline stereo RS	85
6/23/07–6/29/07	1214–1219	Drive; RS	85
6/30/07–8/20/07	1220–1270	Dust storm; Atmospheric dust monitoring; Limited activity to conserve power	85
8/21/07–9/3/07	1271–1284	Drive toward rim of "Victoria crater"; Self Portrait; RS	85–86
9/4/07–9/8/07	1285–1288	Drive toward ingress point; RS; Diagnostics	86
9/9/07	1289	Drive to "Paulo's Perch"; RS	86
9/10/07	1290	Atmospheric RS	86
9/11/07	1291	Toe dip (drive into and out of "Victoria crater")	86
9/12/07–9/13/07	1292–1293	Drive into Victoria crater; RS	86
9/14/07–9/17/07	1294–1297	Odyssey safe mode; RS	86
9/18/07	1298	Odyssey safe mode; Drive toward "Alpha Layer"	86
9/19/07–9/21/07	1299–1301	Atmospheric RS	86
9/22/07–9/25/07	1302–1305	Approach "Alpha Layer"; RS	86
9/26/07	1306	RS	87
9/27/07–10/10/07	1307–1320	IDD "Steno" layer; RS	86–87
10/11/07	1321	Drive to second IDD target on "Steno" layer	87
10/12/07–10/18/07	1322–1327	"Steno" layer: IDD and RS "Hall" target	87
10/19/07–10/20/07	1328–1329	Drive toward "Smith" layer; RS	87
10/21/07–10/22/07	1330–1331	Atmospheric RS	87
10/23/07–11/18/07	1332–1358	IDD "Smith" rock outcrop; RS "Sharp" sequence of fine layers; Targeted RS; RAT diagnostics	87
11/19/07–11/22/07	1359–1361	IDD "Smith2" rock outcrop; RAT diagnostics	87

Table 2. (continued)

Earth Date[b]	Sol	Activity	Site
11/23/07–12/10/06	1362–1379	Continue IDD "Smith2" rock outcrop	87
12/11/07–12/12/07	1380–1381	Atmospheric RS	87
12/13/07	1382	Drive to "Lyell" layer, "Newell" target; RS	87
12/14/07	1383	Atmospheric RS	88
12/15/07–12/25/07	1384–1394	IDD "Lyell_1" target; RS	88
12/26/07	1395	IDD "Lyell_2" target; RS	88
12/27/07–1/2/08	1396–1401	IDD "Lyell_3" target; RS	88
1/3/08	1402	Drive to "Smith-Lyell" contact; RS	88
1/4/08	1403	RS	88
1/5/08	1404	IDD "Smith Lyell" contact; RS	88
1/6/08–1/7/08	1405–1406	IDD "Lyell_4" target; RS	88
1/8/08–1/11/08	1407–1410	IDD diagnostics; IDD "Smith_3"	88
1/12/08–1/16/08	1411–1415	IDD "Lyell" side of "Smith-Lyell" contact; RS	88
1/17/08–1/19/08	1416–1418	Drive to "Buckland" outcrop	88
1/20/08–1/21/08	1419–1420	Atmospheric RS	88
1/22/08–2/8/08	1421–1437	IDD "Buckland" outcrop; RS	88
2/9/08–2/21/08	1438–1450	Drive to "Gilbert" outcrop; RS; Scuff "Gilbert" outcrop; IDD "Lyell-Exeter" target	88
2/22/08	1451	APXS argon; RS	88
2/23/08–2/25/08	1452–1454	IDD filter and capture magnets; RS	88
2/26/08–2/27/08	1455–1456	IDD "Gilbert A"	88
2/28/09	1457	"Gilbert" outcrop: IDD "Dorsal" target	88–89
2/29/08–3/2/08	1458–1460	DSN transmitter failure; Runout	–
3/3/08–3/5/08	1461–1463	"Gilbert" outcrop: IDD "Dorsal" target	88–89
3/6/08–3/10/08	1464–1468	"Gilbert" location: IDD "Dorsal Tail" target	89
3/11/08–3/14/08	1469–1471	"Gilbert" location: IDD "Dorsal New" target	89
3/15/08–3/16/08	1472–1473	Supperres rimshot; Atmospheric RS	89
3/17/08	1474	Atmospheric RS	89
3/18/08–3/26/08	1475–1483	IDD "Gilbert_RAT" target; RS	89
3/27/08–4/14/08	1484–1502	Drive toward "Cape Verde"; RS	89–90
4/15/08–5/28/08	1503–1544	IDD diagnostics; RS	89
5/29/08–5/30/08	1545–1546	RS "Garrels" panorama and "Williams" target; Atmospheric RS	89
5/31/08–6/14/08	1547–1561	Continue drive toward "Cape Verde"; RS	89–90
6/15/08	1562	Scuff and RS soil	90
6/16/08–6/22/08	1563–1569	Continue drive toward "Cape Verde"; RS	89–90
6/23/08–7/5/08	1570–1581	"Cape Verde" panorama; RAT diagnostics	90
7/6/08–7/24/08	1582–1600	Continue drive toward "Cape Verde"; RS; RAT calibration	89–90
7/25/08	1601	Atmospheric RS	90
7/26/08–7/28/08	1602–1604	Drive (left front wheel) diagnostics	90
7/29/08–7/31/08	1605–1607	RS "Eugene Smith," "Siever," and "McKee" targets and "Cape Verde"; Atmospheric RS	90
8/1/08–8/3/08	1608–1610	Safe mode	90
8/4/08–8/16/08	1611–1622	Exit "Victoria crater"; RS	90
8/17/08	1623	RS "Logan" rock weathering target	90
8/18/08–8/19/08	1624–1625	Continue exit "Victoria crater"; RS	90
8/20/08	1626	RS "Jin" cobble	90
8/21/08	1627	Continue exit "Victoria crater"; RS	90
8/22/08	1628	RS "Barghorn" target	90
8/23/08–8/24/08	1629–1630	Continue exit "Victoria crater"; RS	90
8/25/08	1631	RS "Dawson" and "Eugster" targets	90
8/26/08	1632	Continue exit "Victoria crater"; RS	90
8/27/08	1633	RS	90
8/28/08–8/29/08	1634–1635	Atmospheric RS	90
8/30/08	1636	RS tracks, ripple, and "Isle Royale" target	90
8/31/08–9/1/08	1637–1638	Atmospheric RS	90
9/2/08–9/3/08	1639–1640	RS "Bright Patch Two" target	90
9/4/08	1641	Bump to "Bright Patch"	90
9/5/08–9/7/08	1642–1644	IDD "Victoria" rim sand dune	90
9/8/08–9/10/08	1645–1647	IDD "Victoria" ripple soil	90
9/11/08–9/18/08	1648–1654	Drive toward lee side of ripple; Atmospheric RS	90
9/19/08–9/22/08	1655–1658	Atmospheric RS	90
9/23/08–9/24/08	1659–1660	RS; APXS Argon	90
9/25/08	1661	Drive by "Sputnik crater"	90
9/26/08–10/9/08	1662–1675	Drive toward "Cape Victory" and "Cape Agulhas" on "Victoria crater"; RS "Cape Pillar" and "Cape Victory"	90–91
10/10/08	1676	RS "Savu Sea" bedrock	91
10/11/08–10/13/08	1677–1679	Continue drive toward "Cape Victory" and "Cape Agulhas" on "Victoria crater"; RS "Cape Pillar" and "Cape Victory"	90–91
10/14/08	1680	MTES shake	91
10/15/08	1681	Continue drive toward "Cape Victory" and "Cape Agulhas" on "Victoria crater"; RS "Cape Pillar" and "Cape Victory"	90–91

Table 2. (continued)

Earth Date[b]	Sol	Activity	Site
10/16/08–10/17/08	1682–1683	Drive toward "Endeavour crater"; RS	91
10/18/08–11/17/08	1684–1713	Continue drive toward "Endeavour crater"; RS; APXS Argon	91–92
11/18/08–11/22/08	1714–1718	Arrive at solar conjunction location; IDD "Santorini" cobble	94
11/23/08–11/25/08	1719–1721	"Santorini" Panorama; RS "Corfu" outcrop patch	94
11/26/08–11/27/07	1722–1723	Runout	94
11/28/08–12/15/08	1724–1740	Solar Conjunction; IDD "Santorini" cobble	94
12/16/08–12/17/08	1741–1742	Delete data products; Atmospheric RS; IDD "Santorini" cobble	94
12/18/08–12/22/08	1743–1747	IDD and RS "Santorini" cobble	94
12/23/08	1748	Approach "Crete" bedrock and soil targets	94
12/24/08–12/25/08	1749–1750	Atmospheric RS	94
12/26/08–12/28/08	1751–1753	IDD "Crete" bedrock target	94
12/29/08	1754	"Crete" bedrock: IDD "Candia" rock target	94
12/30/08–1/2/09	1755–1758	"Crete": IDD "Minos" soil target	94
1/3/09–1/5/09	1759–1761	Atmospheric RS	94
1/6/09–1/12/09	1762–1767	RAT diagnostics; Atmospheric RS	94
1/13/09	1768	MTES shake test	94
1/14/09	1769	RS; APXS Argon	94
1/15/09	1770	Drive toward "Ranger crater"	94
1/16/09	1771	MTES shake test	94
1/17/09–1/20/09	1772–1775	Atmospheric RS	94
1/21/09	1776	Approach "Ranger crater"	94
1/22/09–1/24/09	1777–1779	RS "Ranger crater"; Atmospheric RS	95
1/25/09–1/26/09	1780–1781	Drive south; RS; APXS Argon	95
1/27/09	1782	Drive by "Surveyor crater"; RS	95
1/28/09	1783	RS; APXS Argon	95
1/39/09	1784	RS ripple offset	95
1/30/09–2/1/09	1785–1787	Drive; RS; APXS Argon	95
2/2/09–2/4/09	1788–1790	PMA fault diagnostics	96
2/5/09–2/14/09	1791–1799	Drive toward "Endeavour crater"; RS; APXS Argon	97
2/15/09	1800	Right front wheel diagnostic drive	98
2/16/09	1801	Automatic AutoNav Map Load Test	98
2/17/09–2/23/09	1802–1808	Continue drive toward "Endeavour crater"; RS; APXS Argon	98
2/24/09	1809	"Marsquake" observation	98
2/25/09	1810	RS; APXS Argon	98
2/26/09	1811	FSW R9.3 build	98
2/27/09–3/4/09	1812–1817	Continue drive toward "Endeavour crater"; RS; APXS Argon	98
3/5/09	1818	RS cobble	98
3/6/09–3/9/09	1819–1822	RS; APXS Argon	99
3/10/09	1823	Bump to "Resolution crater"; RS	99
3/11/09	1824	Approach "Cook_Islands" outcrop	99
3/12/09–3/18/09	1825–1831	Approach, IDD, and RS "Cook Islands" cobble patch; RS "Lost" cobble; Atmospheric RS	99
3/19/09–4/6/09	1832–1849	"Cook Islands" cobble patch: IDD "Penrhyn" and "Takutea" targets	99
4/7/09–4/9/09	1850–1852	Drive to and RS "Adventure" crater	99
4/10/09	1853	Atmospheric RS	99
4/11/09	1854	Drive to "Discovery crater"	99
4/12/09	1855	Atmospheric RS	99
4/13/09–4/15/09	1856–1858	Drive to and RS "Pembroke crater"	99
4/16/09–5/2/09	1859–1874	Continue drive toward "Endeavour crater"; RS; APXS Argon	99–100
5/3/09	1875	"Marsquake" observation	100
5/4/09	1876	RS	100
5/5/09–5/11/09	1877–1883	Bump to pebble patch; IDD and RS "Tilos," "Kos," and "Rhodes" pebbles	100
5/12/09–5/18/09	1884–1890	Drive to and IDD "Kasos" pebble	100
5/19/09–5/26/09	1891–1898	Continue drive toward "Endeavour crater"; RS; APXS Argon	100–101
5/27/09	1899	MI sky flats test	101
5/28/09–6/10/09	1900–1912	Continue drive toward "Endeavour crater"; RS; APXS Argon	102
6/11/09–6/15/09	1913–1917	Atmospheric RS	103
6/16/09–6/17/09	1918–1919	IDD "Ios" target	103
6/18/09–6/24/09	1920–1926	Drive to and IDD "Tinos" target; RS "Donousa," "Dryma," "Naxos," and "Mykonos" targets	103
6/25/09–6/28/09	1927–1930	Continue drive toward "Endeavour crater"; RS; APXS Argon	103
6/29/09–7/9/09	1931–1941	IDD "Little Beach" and "Absecon" targets	103
7/10/09–7/16/09	1942–1947	Continue drive toward "Endeavour crater"; RS	103–104
7/17/09	1948	Marsquake observation; RS	104
7/18/09	1949	RS; APXS Argon	104
7/19/09	1950	Drive to "Kaiko" and "Nereus" craters; RS	104
7/20/09	1951	RS	104
7/21/09–7/30/09	1952–1961	Drive toward "Block Island" meteorite; IDD and RS	104–105
7/31/09–8/10/09	1962–1972	"Block Island" meteorite: IDD and RS "New Shoreham," "Clayhead Swamp," "Springhouse Icepond," "Middle Pond"	105
8/11/09–8/12/09	1973–1974	Bump to "Vail Beach" soil pebbles; IDD "Vail Beach"	105

Table 2. (continued)

Earth Date[b]	Sol	Activity	Site
8/13/09–8/31/09	1975–1992	Bump to "Siah's Swamp" and "Veteran's Park" targets: IDD and RS; IDD and RS "Siah's Swamp2" and "Fresh Pond"; RS "Block Island" meteorite	105
9/1/09–9/2/09	1993–1994	Runout	105
9/3/09–9/4/09	1995–1996	RS	105
9/5/09–9/11/09	1997–2003	Drive around and image "Block Island" meteorite (6 positions), RS	105
9/12/09–9/18/09	2004–2010	Continue drive toward "Endeavour crater"; RS; APXS Argon	105
9/19/09	2011	RS "Nautilus" crater	106
9/20/09–9/21/09	2012–2013	Continue drive toward "Endeavour crater"; RS	106
9/22/09–9/24/09	2014–2015	RS Gjoa crater	106
9/25/09	2016	IDD "Limnos" target	106
9/26/09	2017	Continue drive toward "Endeavour crater"; RS	106
9/27/09	2018	"Marsquake" observation	106
9/28/09–9/30/09	2019–2021	Continue drive toward "Endeavour crater"; RS; APXS Argon	106–107
10/1/09	2022	RS "Shelter Island" meteorite	107
10/2/09	2023	RS; APXS Argon	107
10/3/09–10/12/09	2024–2033	Approach, IDD, and RS "Shelter Island" meteorite: "Dering Harbor" target	107
10/13/09–10/17/09	2034–2038	Drive to "Mackinac" meteorite; RS	107
10/18/09–10/22/09	2039–2043	RS; APXS Argon	107
10/23/09	2044	DSN station down, Runout	108
10/24/09–10/25/09	2045–2046	Continue drive toward "Endeavour crater"; RS	108
10/26/09	2047	RS "Trinidad" crater	108
10/27/09–11/3/09	2048–2054	Continue drive toward "Endeavour crater"; RS; APXS Argon	108
11/4/09–11/12/09	2055–2063	Drive toward "Marquette Island" rock; RS	109
11/13/09	2064	RS	109
11/14/09–11/20/09	2065–2071	"Marquette Island" rock: IDD "Peck Bay" target	109
11/21/09–12/4/09	2072–2085	"Marquette Island" rock: IDD "Islington Bay" target	109
12/5/09–12/7/09	2086–2088	Drive toward "Marquette Island's" unseen side	109
12/9/09–12/12/09	2089–2092	"Marquette Island" rock: IDD "Loon Lake" target	109
12/13/09–12/16/09	2093–2096	RS	109
12/17/09–1/10/10	2097–2121	"Marquette Island" rock: IDD "Peck Bay" target	109
1/11/10–1/13/10	2122–2124	Continue drive toward "Endeavour crater"; RS	109
1/15/10–1/19/10	2125–2129	Drive toward "Concepciòn" crater	109–111
1/20/10	2130	AEGIS checkout	110
1/21/10–1/28/10	2131–2138	Continue drive toward "Concepciòn" crater	109–111
1/29/10	2139	RS	111
1/30/10	2140	"Concepciòn" panorama	111
1/31/10	2141	IDD "Mahany Island" target	111
2/1/10	2142	"Concepciòn" panorama	111
2/2/10–2/3/10	2143–2144	IDD "Loboc River" target	111
2/4/10–2/7/10	2145–2148	Drive toward "Concepciòn crater"	111
2/8/10	2149	Bump toward "Chocolate Hills"	111
2/9/10–2/10/10	2150–2151	"Chocolate Hills" rock: IDD "Aloya" dark material	111
2/11/10	2152	Bump around "Chocolate Hills"	111
2/12/10–2/14/10	2153–2155	"Chocolate Hills" rock: IDD "Arogo" target	111
2/15/10	2156	RS	111
2/16/10–2/19/10	2157–2160	"Chocolate Hills" rock: IDD "Tears" target, IDD "Dano" target	111
2/20/10–3/3/10	2161–2171	Drive around "Concepciòn crater"; RS	111
3/4/10	2172	AEGIS checkout	111
3/5/10–3/8/10	2173–2176	Continue drive around "Concepciòn crater"; RS	111
3/9/10	2177	Return to "Pink Path" and drive to "Endeavour crater"	111
3/10/10–3/27/10	2178–2195	Continue drive toward "Endeavour crater"; RS	111–112
3/28/10–3/30/10	2196–2198	RS "San Antonio West" and "San Antonio East" craters	114
4/1/10–4/12/10	2199–2210	Continue drive toward "Endeavour crater"; RS	114
4/13/10	2211	Dune crossing, soil mechanics experiment	115
4/14/10–4/22/10	2212–2220	Continue drive toward "Endeavour crater"; RS	115
4/23/10	2221	AEGIS watch	115
4/24/10–4/25/10	2222–2223	RS	116
4/26/10	2224	IDD "Ocean Watch" undisturbed soil target	116
4/27/10–4/29/10	2225–2227	Continue drive toward "Endeavour crater"; RS	116
4/30/10–5/2/10	2228–2230	Drive toward "Newfoundland" rock; RS	116
5/3/10–5/13/10	2231–2240	Continue drive toward "Endeavour crater," drive to "Lily Pad"; Argon APXS, drive to "Lily Pad"; RS	116
5/14/10–5/19/10	2241–2246	RS; MarsQuake Experiment; Drive south	116–117
5/20/10–5/26/10	2247–2253	AEGIS experiment; Drive east; RS	117
5/27/10–5/29/10	2254–2256	Drive; RS	117
5/30/10–5/31/10	2257–2258	Get fine attitude; recharge; Mini-TES in stand down mode	117–118
6/1/10–6/3/10	2259–2261	PMA diagnostics	118
6/4/10–6/6/10	2262–2264	Hazcam; Argon APXS; Recharge	118
6/7/10	2265	PMA diagnostics	118
6/8/10–6/9/10	2266–2267	RS; Recovery QFA and postdrive imaging	118
6/10/10–6/17/10	2268–2274	RS; Recharge; Drive east toward Endeavour	118

Table 2. (continued)

Earth Date[b]	Sol	Activity	Site
6/18/10–6/19/10	2275–2276	RS; Drive south	118
6/20/10–6/21/10	2277–2278	Argon APXS; AEGIS experiment	119
6/22/10–6/30/10	2279–2287	Drive east-southeast, drive northward, drive east; RS	120
7/1/10–7/5/10	2288–2292	Drive eastward; RS; AEGIS experiment	120
7/6/10–7/7/10	2293–2294	Drive east toward "Endeavour crater"; RS	120
7/8/10–7/9/10	2295–2296	Drive; RS	120
7/10/10	2297	IDD "Juneau_Road_Cut" target, IDD "Juneau" target	120
7/11/10	2298	RS	120
7/12/10–7/13/10	2299–2300	Drive east-southeast toward gravel pile; RS	120–121

[a]RS, remote sensing; MEX, Mars Express; AEGIS was an experiment focused on automatic rock detection. Other acronyms defined in Table 1.
[b]Read Earth Date 7/1/05–7/4/05 as 1–4 July 2005, etc.

2250, after bypassing several fields of purgatoids, Opportunity was able to start traversing southeast, directly toward the rim of Noachian-aged Endeavour crater, with the intent of exploring the ancient rocks exposed on the crater's rim.

[13] The initial primary science target for Opportunity, after leaving Purgatory, was Erebus, a ~220 m wide, degraded impact crater with ripples surrounding the crater and occupying most of the crater floor (Figure 2). Extensive remote sensing and in situ measurements were made on the Olympia outcrop on the northwestern side of Erebus crater. Detailed remote sensing data were also acquired for the Payson outcrops located on the southwestern side of Erebus. The Jammerbugt ripple was another location in which significant wheel sinkage and slippage were encountered. Opportunity backed out of this ripple on sol 841, after six sols of extrication. Several rock and soil targets, along with small craters, were then examined during traverses to Victoria crater. Opportunity reached Victoria's crater rim on sol 953.

[14] The first part of the Victoria campaign focused on remote sensing of crater walls, done by driving to promontories and acquiring Pancam and Navcam mosaics of adjacent cliff faces, together with acquiring data for cobbles strewn onto the smooth annulus surrounding the crater (Figure 2). This phase focused on the northwestern quadrant of the crater and extended from sols 953 to 1290. After determining that Duck Bay was a reasonable location to enter the crater and make measurements of Burns formation rock targets as a function of depth, Opportunity entered Victoria on sol 1292 and stayed in the crater, acquiring detailed remote sensing and in situ observations. Opportunity exited Duck Bay on sol 1622. After soil measurements on the annulus surrounding Victoria, and additional remote sensing of the crater walls, Opportunity on sol 1682 began traverses toward Endeavour crater, located ~20 km to the southwest of Victoria.

[15] During the post-Victoria traverses Opportunity encountered a number of impact craters and a variety of cobbles and boulders, discussed in detail in a subsequent portion of this paper. Key to successful traversing has been the avoidance of purgatoids, using Mars Reconnaissance Orbiter HiRISE images [*McEwen et al.*, 2007] and Odyssey THEMIS-based thermal inertia maps [*Christensen et al.*,

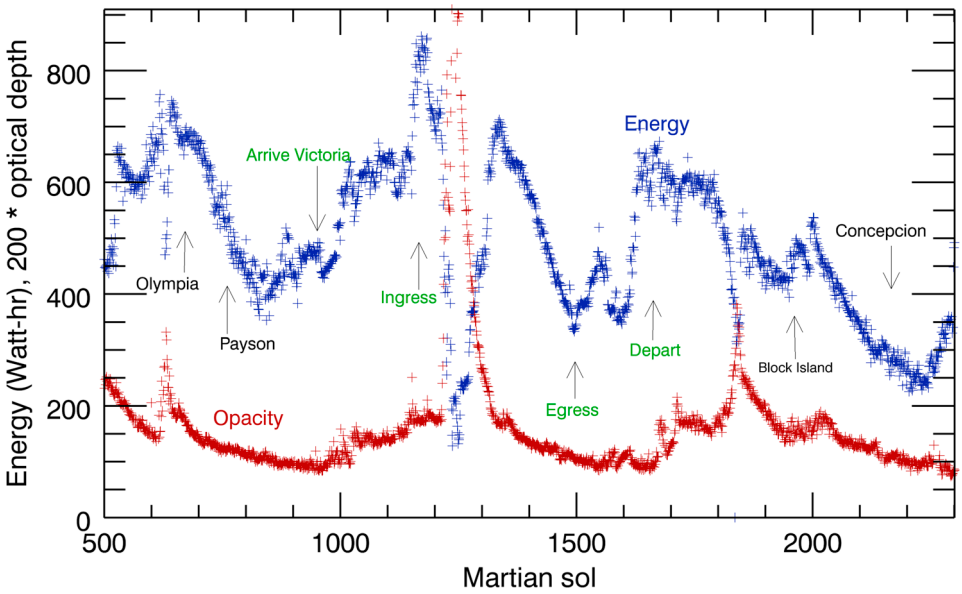

Figure 3. Time series available rover energy, atmospheric opacity, and major events for Opportunity from sol 511 to sol 2300. Opacity at 880 nm is shown multiplied by a factor of 200.

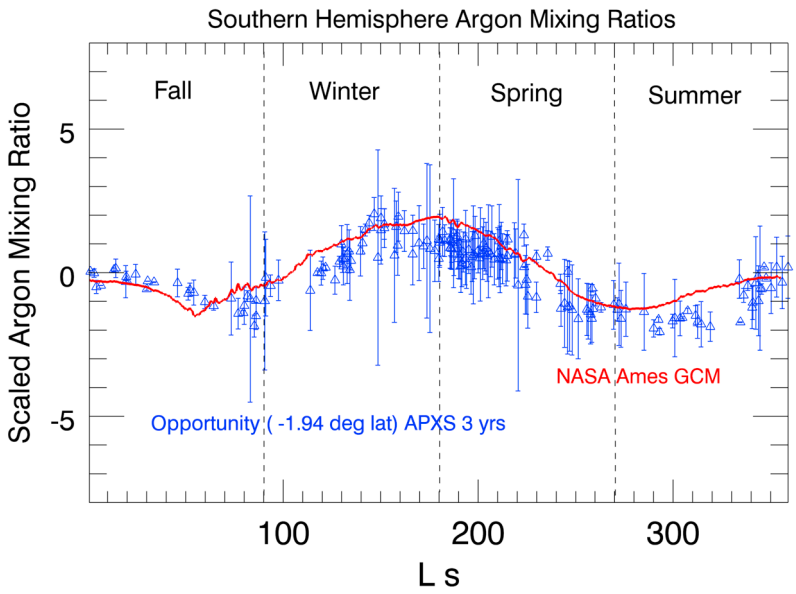

Figure 4. Scaled volume mixing ratios of argon to carbon dioxide are shown for three years of Opportunity APXS observations of the atmosphere together with mixing ratios derived from the NASA Ames general circulation model. Both data sets have been scaled by subtracting means and dividing by standard deviations. The southern winter solstice occurs at $L_s = 90°$, whereas the northern winter solstice occurs at $L_s = 270°$. See text for explanation of trends.

2004a; *Fergason et al.*, 2006], together with extensive rover-based remote sensing observations, to drive along paths that minimized traverses across large ripples [*Parker et al.*, 2010]. This led to a southern to southwestern path south from Victoria to avoid the purgatoid fields, and then turning to the southeast on a more direct route to the rim of Endeavour (Figure 2).

4. Modern Atmospheric Processes

[16] In addition to addressing the primary mission themes of characterizing past environmental conditions, and the role of water in formation and alteration of crustal materials, Opportunity has continued to make periodic measurements that pertain to current atmospheric characteristics and dynamics. Pancam has been used on a sol-by-sol basis to determine atmospheric opacity at wavelengths of 440 and 880 nm. This activity has supported mission operations tactically by providing estimates of available solar irradiance on the panels. When combined with orbital observations, the Pancam measurements have been critically important for tracking dust storms and the impact on vehicle performance and safety. Regional dust storms have been observed during each summer season, with a planet-encircling event occurring during the early summer of the third year of operations (~sols 1200–1300, see Figure 3). This led to an available energy of less than 200 Wh and placed Opportunity in a survival mode. Occasional dust devils have been imaged by Opportunity and repeated coverage of the plains surrounding Opportunity by the Mars Reconnaissance Orbiter's Context Imager (CTX) [*Malin et al.*, 2007] showed a number of ephemeral dust devil tracks. Wind directions and magnitudes were found by inspection of aeolian streaks, and mesoscale modeling of atmospheric circulation models, to vary during the course of the Martian year [*Sullivan et al.*, 2005; *Jerolmack et al.*, 2006; *Geissler et al.*, 2010; M. Chojnacki et al., Orbital observations of contemporary dune activity in Endeavour crater, Meridiani Planum, Mars, submitted to *Journal of Geophysical Research*, 2011].

[17] Winter atmospheric measurements for science have focused on sky imaging to detect the well-known winter aphelion water ice cloud "belt" [e.g., *Clancy et al.*, 1996]. Fewer clouds were observed during the three periods near aphelion than would have been predicted from Earth-based and orbital observations [i.e., *Wolff et al.*, 1999]. The paucity of clouds suggests that the meteorology of the Meridiani region may be more complex (and thus more interesting) than previously understood.

[18] When not in use to measure compositions of rocks and soils, and when rover energy permitted, APXS has been used to monitor seasonal and interannual variations in atmospheric argon contents (Figure 4). The argon mixing ratio is a tracer for atmospheric transport because it is a noncondensable gas under Martian conditions. On the other hand, the carbon dioxide content of the atmosphere varies significantly as a function of season because it condenses over the winter pole to form the seasonal ice cap. The southern winter is longer and colder than the northern winter season because the southern winter season occurs near aphelion. The southern pole is also topographically higher than the northern pole. Consequently, the southern winter carbon dioxide cap is more extensive than the northern winter cap. These dynamics are evident in global pressure variations recorded by the Viking Landers, with lowest surface pressures associated with the southern winter [*Tillman et al.*, 1993].

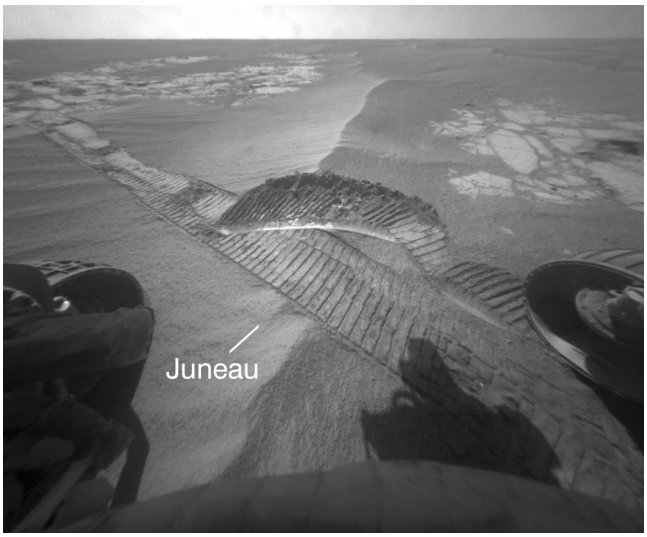

Figure 5. Front Hazcam image looking to the north showing a drive and turn in place across the crest of a ripple. Outcrop is shown as bright polygonal regions on either side of the ripple. Juneau is the location of an Instrument Deployment Device (IDD) target on the western flank of the ripple. Microscopic Imager (MI) data for Juneau show that it is covered with a dense array of hematitic concretions (Figure 6). Front Hazcam frame 1F331928037RSLAKVTP1214L0MZ acquired on sol 2295.

[19] *Sprague et al.* [2007] reported global variations in argon mixing ratios using Odyssey gamma ray spectrometer data, focusing on the sixfold argon enhancement during the winter over the southern polar region (−75 to 90° latitude). Argon mixing ratios were found to peak over the south pole at L_s = 90 degrees and then undergo a rapid decline to lowest values by the southern summer (L_s = 270 degrees). Argon mixing ratios for an adjacent latitude band (−60 to 75 degrees latitude) showed a similar pattern, but shifted to a slightly later time. Argon was not found to concentrate above the north polar winter cap. These patterns were interpreted as evidence for meridional transport of argon with carbon dioxide as part of the global atmospheric circulation system, particularly combined with relatively weak south pole to equator transient eddies that cause buildup of argon over the winter cap [*Nelli et al.*, 2007].

[20] Opportunity-based argon atmospheric mixing ratios show minimum values at L_s = 90 degrees (beginning of the southern winter), during the period when argon shows the highest concentration over the growing south polar seasonal cap (Figure 4). The Opportunity-based argon mixing ratios increase rapidly as the south polar concentrations decrease. Peak Opportunity-based values are reached during late southern winter to early spring seasons. Argon mixing ratios then start decreasing, reaching a broad low between 270 to 320 degrees L_s (northern winter season). The overall trends were simulated with the NASA Ames global circulation model, which reproduced the broad patterns discussed above, including the sharp decrease and increase in Opportunity-based values associated with the south polar winter cap formation and sublimation. The broad low associated with formation and sublimation of the northern winter cap is also reproduced. The model fit to the data shows temporal offsets and there are also interannual variations in Opportunity-based argon mixing ratios. The differences between the model and the interannual variations are currently study topics. It is clear that the Opportunity data provide quantitative "ground truth" for use with Odyssey-based argon mixing ratios as tracers for atmospheric circulation, along with "ground truth" validation of global circulation models.

5. Aeolian Ripples and Mobility Issues

5.1. Nature and Origin

[21] The plains surfaces traversed by Opportunity are largely covered by aeolian ripples that have crests predominantly oriented in a north to south direction. Hematitic concretions are concentrated on the ripple crests, whereas interiors are dominated by a mix of basaltic sand, hematitic concretions, and dust [*Christensen et al.*, 2004b; *Soderblom et al.*, 2004; *Sullivan et al.*, 2005; *Arvidson et al.*, 2006; *Jerolmack et al.*, 2006]. Opportunity's remote sensing measurements during traverses and stops for in situ measurements during the period covered by this paper show a change to larger ripples and a greater areal exposure of outcrops, beginning ~280 m south of Purgatory ripple (Figure 2). This change corresponds to a boundary between a relatively uniformly dark, high thermal inertia surface covered by relatively small ripples to the north, to a mix of bright and dark surfaces to the south (Figure 2). The darker surfaces south of the boundary, which are dominated by ripples, have low thermal inertias relative to the surrounding brighter surfaces, which are dominated by bedrock exposures. South of Victoria fields of large ripples (i.e., purgatoids) identified using HiRISE images were avoided during traverses by initially traversing to the southwest, then south, and finally back to the southeast [*Parker et al.*, 2010].

[22] Detailed in situ measurements of ripple surfaces and interiors collected throughout the Opportunity mission provide key information on the nature and extent of these aeolian features. For example, on sol 2297, at the end of a drive, Opportunity turned to maximize UHF communication rates. The turn caused the right front wheel to cut into the crest of a ripple, exposing the upper part of the interior (Figure 5). MI data were acquired for the excavated materials and an undisturbed surface target, Juneau, on the western flank of the ripple. The Juneau images show a high areal concentration of hematitic concretions (Figure 6), consistent with prior observations of ripple surfaces (Figures 7). Specifically, application of correspondence analysis [e.g., *Arvidson et al.*, 2006, 2008, 2010] and comparison to MI data show that the compositional trends associated with factor 1 loadings range from basaltic sand samples (e.g., Auk target within Endurance crater) as one end-member, to almost complete areal coverage by hematitic concretions (e.g., Juneau) as the other end-member. In fact, the location of samples along this mixing line (i.e., factor 1 loading in Figure 7) is predicted with high fidelity based on the areal fraction of concretion coverage. A minor, but important direction (factor 2 loading shown in Figure 7) delineates targets with enhanced sulfur and chlorine. MI data for these samples show the presence of fine-grained materials (e.g., Les Houches, Figure 6). These fine-grained targets are found

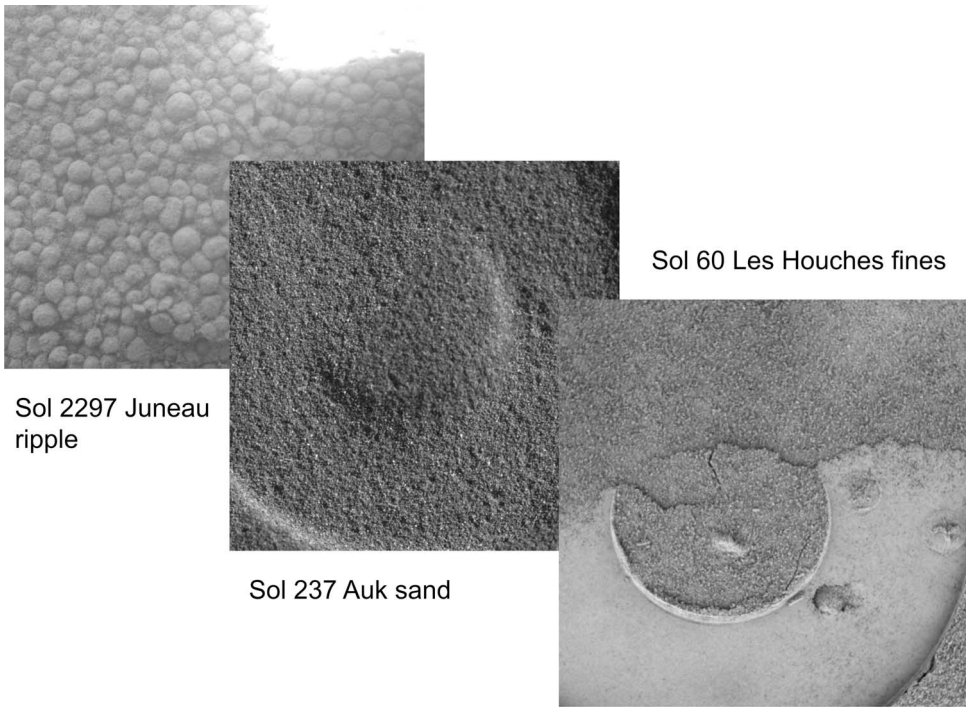

Figure 6. Series of MI images, each 3 cm across, of soils encountered during Opportunity's traverses. Juneau is a ripple surface dominated by hematitic concretions. Auk sand was encountered in Endurance crater, whereas the fine-grained dust target, Les Houches, was found on the perimeter of Eagle crater. These targets form compositional end-members in the APXS data, as shown in Figure 7.

adjacent to Eagle (sol 60 data), Endurance (sol 123), and Victoria (sol 1647) craters and include dust likely deposited in or near the craters in local aeolian traps.

[23] Ripples within the regions traversed by Opportunity have a dominant strike of north-south, based on examination of HiRISE data and azimuths measured from Pancam and Navcam data (Figures 8–10). The Raleigh crater (Figure 9) is part of the Resolution crater cluster, a group of small impact craters spread over an area of ~120 m by 80 m, and is located to the south of Victoria (Table 2). Raleigh (and others within the cluster) must have formed after the last major phase ripple migration ceased, since the crater cuts across the ripples and exposes layers perpendicular to the ripple crest (Figure 9) [*Golombek et al.*, 2010]. These exposures provide important information about the wind direction that produced the ripple fields. The layers dip slightly toward the west. This pattern is consistent with ripple formation by easterly winds in which sand was trapped on the leeward faces and the ripple migrated over the deposits, producing layers that dip slightly toward the leeward direction. The concentration of hematitic concretions on crests is due to the fact that these relatively large grains travel in creep or traction mode and are left behind as the sand saltates in the wind direction. Currently the dominant sediment-moving winds vary in azimuth over time [e.g., *Geissler et al.*, 2010; M. Chojnacki et al., submitted manuscript, 2011] and seem to have produced a set of subsidiary ripples and serrated the older, larger ripple crests, depositing fine-grained materials within and on the large north-south oriented ripples (e.g., Figure 10). This trapping of fine-grained material is inferred to have produced surfaces with slightly lower thermal inertias as compared to surrounding bedrock or smaller ripples.

[24] On a regional scale in Meridiani Planum low thermal inertia streaks are common and extend to the west and northwest from craters and other topographic obstacles, including the locations of the large ripples to the west and northwest of Endeavour crater (Figure 11). These low-temperature streaks have remained invariant during the 2002 to 2010 observation period of the Odyssey THEMIS IR observations and are interpreted to have been produced by easterly to southeasterly winds. Global circulation models that simulate the modern climate of Mars do not produce strong easterlies within the latitudes that include Meridiani Planum [*Fenton and Richardson*, 2001; *Haberle et al.*, 2003]. Indeed, observations of fresh impact craters seen by Opportunity and HiRISE indicate that the latest major phase of ripple migration occurred between ~50,000 to 200,000 years [*Golombek et al.*, 2010]. During earlier periods of time, when the spin axis of Mars was at a higher orbital obliquity than the current value of 25 degrees, the solstice Hadley cell circulation would have occupied a wider latitudinal belt and very likely produced strong easterlies that generated the north-south oriented ripples observed by Opportunity. In fact, modeling of obliquity changes shows that the obliquity can vary by 20° over a time scale of hundreds of thousands of years [e.g., *Ward and Rudy*, 1991], a timing consistent with the last major ripple migration period as discussed above.

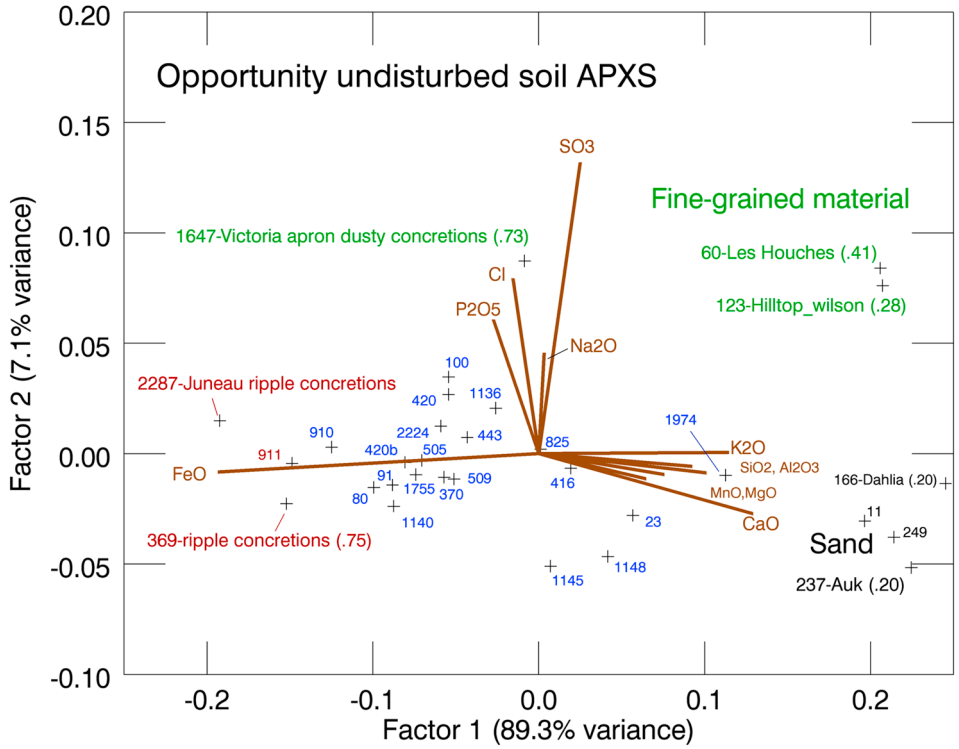

Figure 7. Correspondence analysis plot showing all undisturbed soil targets (labeled by sol) for which APXS data were acquired. Numbers in parentheses correspond to the ratio of ferric to total iron for the targets based on MB observations. The primary trend is from basaltic sands on the right side of the diagram to high concentrations of hematitic concretions on the left. Targets with enrichments in dusty material map separately from the dominant sand to concretion "mixing line." Iron oxidation states are consistent with the inferred mineralogy, with higher values for targets with a higher abundance of hematitic concretions.

5.2. Mobility Issues

[25] Crossing ripples with wavelengths larger than Opportunity's wheel base has occasionally proven to be problematic, leading to embedding at the Purgatory and Jammerbugt ripples, and causing excessive wheel sinkage and slippage as recently as sol 2220 (Table 2 and Figures 12–13). These mobility difficulties occurred while Opportunity attempted to drive up and over ripple flanks. To provide a quantitative evaluation of these mobility difficulties a 200 element dynamical model of Opportunity was constructed in software, including wheel-soil interactions with wheel sinkage and slippage into deformable soils. This software was built on the framework developed for modeling Spirit and its proposed extrication drives [*Arvidson et al.*, 2010]. Normal and shear stresses between the wheels and soil were modeled using the classical Bekker-Wong terramechanics expressions that describe relationships among normal and shear stresses, applied wheel torque, wheel slip, and wheel sinkage as a function of soil properties [e.g., *Wong*, 2003]:

$$\sigma = \left(k_c/b + k_\varphi\right) z^n \tag{1}$$

$$\tau = (c + \sigma \tan(\varphi))\left(1 - e^{-j/kx}\right) \tag{2}$$

where σ is the normal stress and τ is the shear stress between the wheel and soil, k_c/b is the ratio of soil cohesion moduli to

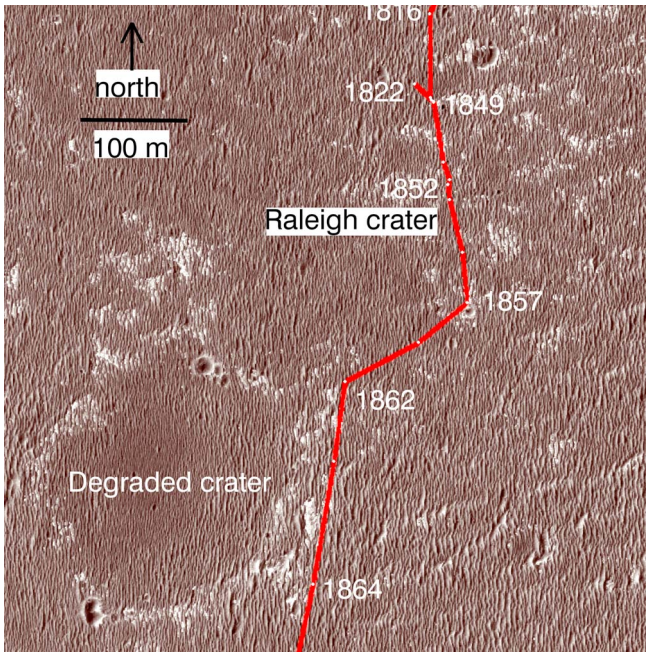

Figure 8. HiRISE view of ripples around Raleigh crater, along with Opportunity's traverses and sols shown for selected positions. Note the bright outcrop and extensive coverage by north-south trending aeolian ripples. Portion of HiRISE frame ESP_016644_1780_red.jp2.

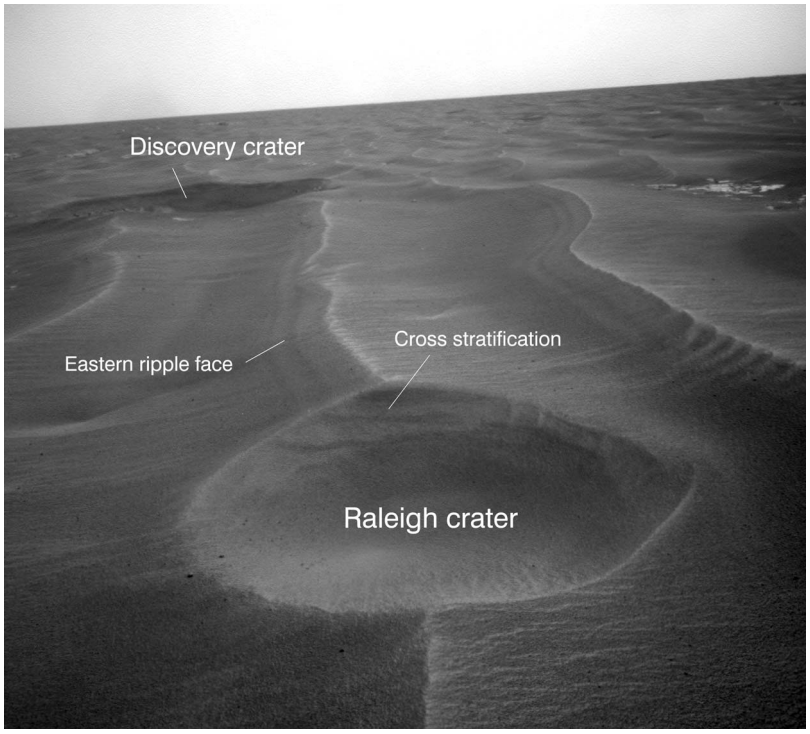

Figure 9. Navcam view looking to the south into the ~2 m wide Raleigh crater. Note the eastern ripple slope exposes light and dark bands that can be extended to the third dimension by noting the cross stratification on the crater wall. Stratification is consistent with formation of ripples by easterly to southeasterly winds, as discussed in the text. Image acquired on sol 1852. Navcam frame 1N292594992RSD99NGP1921L0MZ.

wheel width, k_φ is the internal friction moduli, z is the depth of wheel sinkage, n is a scaling exponent, c is the soil cohesion, φ is the soil angle of internal friction, j is the slip value between the wheel and soil, and k_x is the shear deformation modulus in the longitudinal or drive direction. The value for j is determined based on the magnitude of wheel sinkage into soil.

[26] Increased wheel sinkage due to increased weight over a given wheel generally leads to increased contact area between the wheel and soil and increased compaction resistance, thereby increasing the amount of slippage, S, for a driven wheel as motor torques are increased to compensate:

$$S = (1 - V/R\omega)*100 \quad (3)$$

where V is the longitudinal velocity of the wheel, R is the wheel radius, and ω is the wheel angular velocity. As slippage increases, additional sinkage generally occurs as soil is

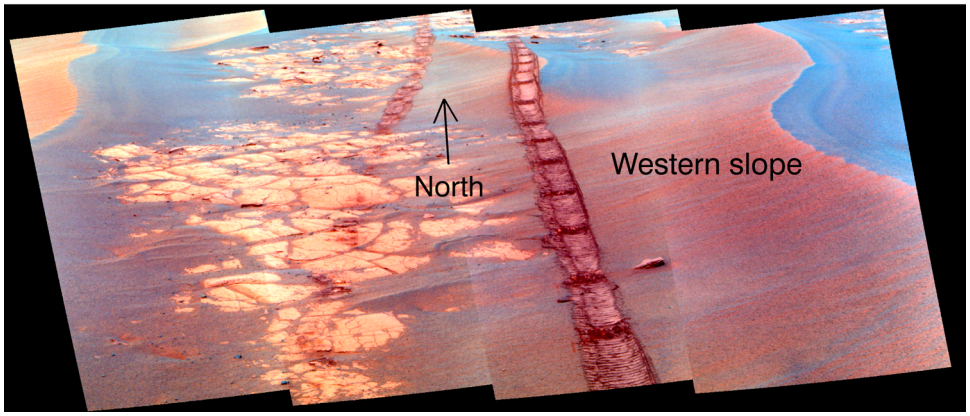

Figure 10. Pancam false color image mosaic looking north and showing the bright red western sides of ripples. Pancam bands L2 (753 nm), L5 (535 nm), and L7 (432 nm) are shown as red, green, and blue. Data acquired on sol 1858, after a major dust storm.

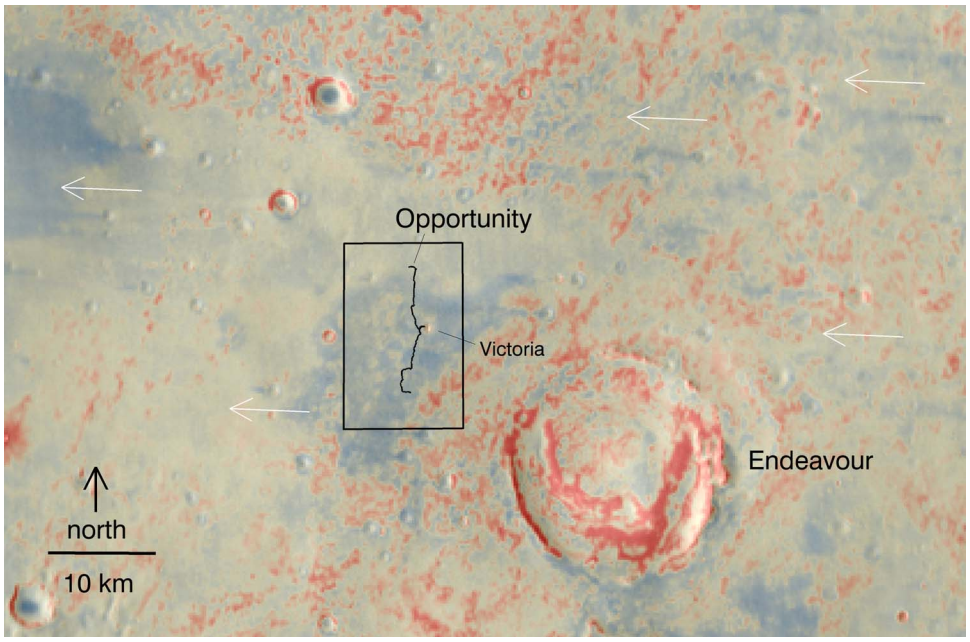

Figure 11. Color-coded predawn THEMIS IR scaled temperature values and Opportunity's traverses overlain onto THEMIS daytime IR mosaic. Arrows show low-temperature streaks extending eastward from craters. Note also the low-temperature zone to the west of Endeavour, including regions traversed by Opportunity. Red colors correspond to terrains with thermal inertias between ~155 and 180 J m^{-2} K^{-1} $s^{-1/2}$ and blue to regions with thermal inertias between ~140 and 145 J m^{-2} K^{-1} $s^{-1/2}$. Box shows region covered in Figure 2. Lower thermal inertia areas are dominated by fields of relatively large ripples that have trapped fine-grained aeolian deposits. Bedrock has slightly higher thermal inertias than ripples.

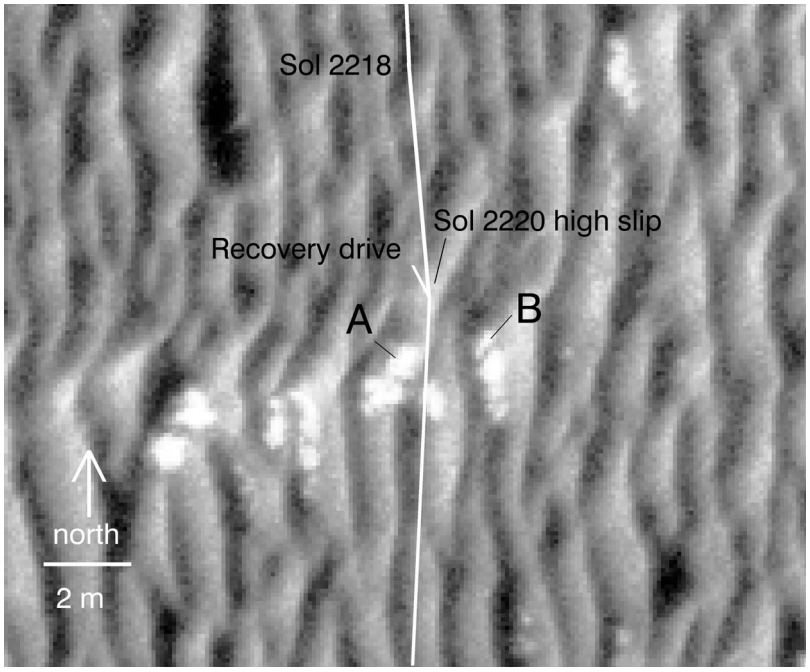

Figure 12. HiRISE view of sol 2220 high slippage and sinkage location on the western side of a ripple. Locations A and B are shown on the Navcam view in Figure 13. Portion of HiRISE frame ESP_016644_1780_red.jp2.

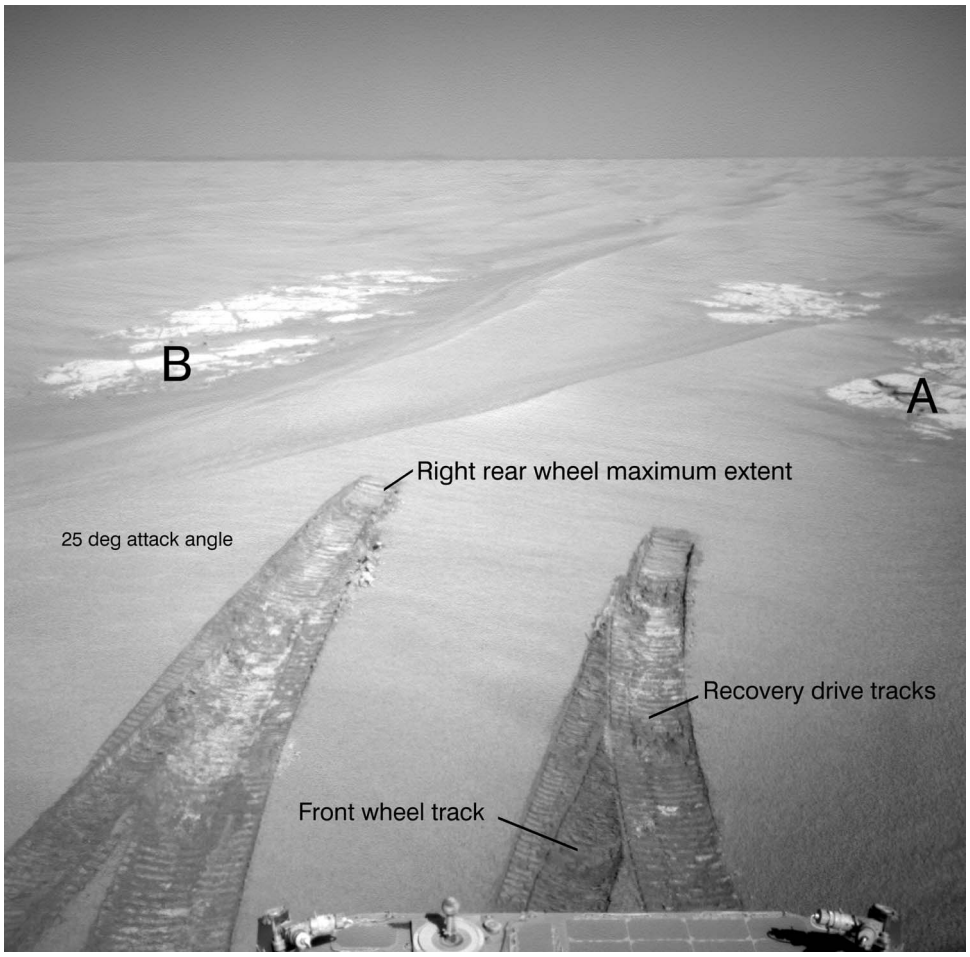

Figure 13. Navcam image acquired on sol 2226 of the sol 2220 high slippage and sinkage location on the western side of a ripple. The shallow angle of attack relative to the ripple crest put all six wheels on the relatively soft soil. During its climb up the ripple, slip equaled 58% and the drive was halted by onboard Visodom software. Navcam frame 1N325805274RSDAG12P19170L0MZ.

moved in the direction of the spinning wheel. This further increases motion resistance as the wheel comes in contact with additional soil during sinkage. At some point the maximum soil shear stress before failure is reached and slippage becomes effectively 100%, causing longitudinal motion to cease.

[27] The sol 2220 drive ended when visual odometry [*Maimone et al.*, 2007] showed ~58% wheel slip, which was above the limit set for continuing the drive. This was a fortuitous event for Opportunity since onboard use of the imaging systems to track slip was done every ~20 m or so during a traverse. The high slip occurred when Opportunity was driving backward and scaling the western side of the ripple at an acute angle (~25°) relative to the ripple crest azimuth, with a rover tilt magnitude of ~8° (Figures 12–13). The ~58% slippage values occurred when six wheels were on the ripple. Wheel sinkage measured from Navcam data taken after extrication from the ripple was ~5 cm. The front wheel (i.e., on the downslope side) tracks show evidence of slip sinkage, based on disruption of the cleat imprints (Figure 13).

[28] To replicate the incipient embedding the Opportunity dynamic element model was set to drive backward on an 8° degree slope into nearly cohesionless soil (c~1 kPa) with an angle of internal friction, φ = 30°, following results from soil trenching experiments conducted by Opportunity earlier in the mission [*Sullivan et al.*, 2010]. Other parameters in equations (1) and (2) were varied to match actual drive results, although detailed sensitivity calculations showed that results were to first-order invariant to the chosen values for k_c. Thus, the modeling focused on varying numerical values of k_φ, n, and k_x. The first two parameters control the amount of static sinkage whereas the third controls the amount of slippage for a given sinkage magnitude. The models replicated observed values of sinkage and slippage with n = 1.1, k_φ = 75,000, and k_x = 65 mm. These values are consistent with the presence of relatively soft soil into which the wheels for the 179 kg Opportunity rover would sink to a few centimeters on flat terrain. Also the value for k_x is toward the upper end of sandy soils for Earth and indicates that relatively high slip values should occur with even modest sinkage and increased compaction resistance. The lesson for mobility was to keep all six wheels from simultaneously being on a ripple flank with the vehicle driving in an uphill direction. During the simulation it was found that the middle and rear wheels bore most of the weight and thus underwent

Table 3. Overview of Cobbles Discussed in This Paper in Order of Discovery

Name[a]	Sol[b]	Classification and Reference[c]	Location	Measurements[d]		
				APXS	MB	MI stacks
Bounce Rock	63	basaltic shergottite [1, 2]	close to the rim of Eagle crater	2U, R	7U, R	10U,4R
Lion Stone	105	outcrop fragment [2, 3]	northwestern rim of Endurance crater	U, R	U, R	2U, 5R
Barberton	121	dark toned cobble (Barberton group) [2, 3, 4, 5]	southern rim of Endurance crater	U	U	2U
Heat Shield Rock	347	iron meteorite [2, 4, 6, 7]	plains; close to the Heat Shield	U, B	U, B	6U, 4B
Russett	381	outcrop fragment [2, 3]	plains	U	U	2U
Arkansas	551	dark toned cobble (Arkansas group) [2, 3]	close to Erebus crater	U	U	U
Perseverance	554	dark toned cobble (Arkansas group) [2, 3]	close to Erebus crater	U	n. a.	U
Antistasi	641	dark toned cobble (Arkansas group) [2, 3]	close to Erebus crater	U	U	4U
JosephMcCoy	886	dark toned cobble (Arkansas group) [2, 3]	Jesse Chisholm area close to Beagle crater	U	U	4U
Haiwassee	886	dark toned cobble (Arkansas group) [2, 3]	Jesse Chisholm area close to Beagle crater	U	n. a.	U
Santa Catarina	1045	dark toned cobble (Barberton group) [2, 3, 4, 5]	Cobble field close to the rim of Victoria crater	U	U	5U
Santa Catarina cobble field	1045	likely genetically related to Santa Catarina [4, 8]	Cobble field close to the rim of Victoria crater	n. a.	n. a.	n. a.
Santorini	1741	dark toned cobble (Barberton group) [2, 3, 5]	~800 m south of Victoria crater	2U	U	3U
Kos	1879	dark toned cobble (Arkansas group) [2]	~1.5 km south of Victoria crater	U	n. a.	U
Tilos	1879	dark toned cobble (Arkansas group) [2]	~1.5 km south of Victoria crater	U	n. a.	U
Rhodes	1879	dark toned cobble (Arkansas group) [2]	~1.5 km south of Victoria crater	U	n. a.	U
Kasos	1886	dark toned cobble (Barberton group) [2, 3, 5]	~1.5 km south of Victoria crater	U	U	4U
Block Island	1961	Iron meteorite [2, 4, 7]	~4 km south-southwest of Victoria crater	6U	4U	26U
Vail Beach	1974	dark toned cobble (Arkansas group) [2, 3]	~4 km south-southwest of Victoria crater	U	n. a.	5U
Shelter Island	2022	Iron meteorite [4, 7]		U	n. a.	2U
Mackinac Island	2034	Iron meteorite [4, 7]		n. a.	n. a.	n. a.
Marquette Island	2065	Martian mafic igneous ejecta block [9]		3U, R	3U, R	5U, 8B, 10R
Chocolate Hills	2150	Impact melt covered ejecta block	on the rim of Concepción crater	U	U	18U

[a]Names are informal and not officially approved by the International Astronomical Union.
[b]The sol indicates the beginning of investigations with IDD instruments.
[c]References: [1], *Zipfel et al.* [2011]; [2], *Weitz et al.* [2010]; [3], *Fleischer et al.* [2010a]; [4], *Schröder et al.* [2008]; [5], *Schröder et al.* [2010]; [6], *Connolly et al.* [2006]; [7], *Ashley et al.* [2010]; [8], *Ashley et al.* [2009]; [9], *Mittlefehldt et al.* [2010].
[d]Number of APXS, Mössbauer (MB) and MI measurements listed for undisturbed (U), brushed (B) and RAT-abraded (R) targets. Number is omitted if one measurement was made.

the most sinkage, thereby significantly increasing compaction resistance. Slippage increased as torque was increased to maintain constant wheel angular velocity, leading to slip sinkage, and exceeding the 58% slippage limit for continuing the drive. Opportunity was able to back out of the ripple with one drive and was then commanded to continue to drive south along an interripple zone until a smaller ripple system was encountered to cross over toward the east.

6. Cobble and Boulder-Sized Rock Fragments

[29] During the mission period covered by this paper Opportunity has characterized a number of individual rock fragments with a variety of sizes. These rocks have been found near craters, in isolated clusters covering small to moderate (tens to hundreds m^2) areas, and sometimes as isolated pebbles, cobbles, or boulders separated by hundreds of meters. For reference, Table 3 lists all rock fragments that were investigated in detail with IDD instruments throughout the mission. Many additional cobble-sized and smaller rock fragments have been characterized with Pancam, Navcam, and/or Hazcam observations [e.g., *Weitz et al.*, 2010]. These observations are not listed in Table 3.

[30] Five basic types of rock fragments were found and characterized in detail during Opportunity operations: (1) local impact ejecta that consist of sulfate-rich sedimentary material (e.g., Chocolate hills, Figures 14–15); (2) basaltic materials that are likely impact ejecta fragments (e.g., Bounce Rock) from distant sources; (3) rock fragments that are a mix of sulfate and basaltic materials that are likely impact melt products (e.g., Arkansas); (4) stony-iron meteorites (e.g., Barberton); and (5) iron-nickel meteorites (e.g., Block Island, Figure 16).

[31] Chocolate Hills is an ejecta fragment from Concepción crater, a ~10 m wide, relatively fresh impact crater located on the plains to the south of Victoria (Figures 2, 14, and 15). This rock is a finely layered, sulfate-rich material with hematitic concretions. The rock is partially coated with a mix of basaltic sand and hematitic concretions cemented by fine-grained hematite, based on analysis of MI, APXS, and MB data. The coating is interpreted to be a fracture filling deposit similar in origin to the fins found in Victoria crater and previous locations [*Knoll et al.*, 2008]. Fins are indurated, fracture filling materials that are now raised features due to differential aeolian erosion of the surrounding softer sulfate-rich rocks. The presence of hematite implies that aqueous processes have been operative at least episodically since formation of the sulfate-rich sandstones that underlie Meridiani Planum.

[32] Bounce Rock was encountered just outside of Eagle crater and is rich in pyroxene, with a composition similar to the basaltic shergottite class of Martian meteorites [*Zipfel et al.*, 2011]. A possible source for this ejecta fragment is the ~20 km diameter Bopolu crater, located ~75 km to the southwest of Eagle crater (Figure 1). The boulder Marquette Island was encountered during a traverse on the plains located to the south of Victoria crater (Table 2) [*Mittlefehldt*

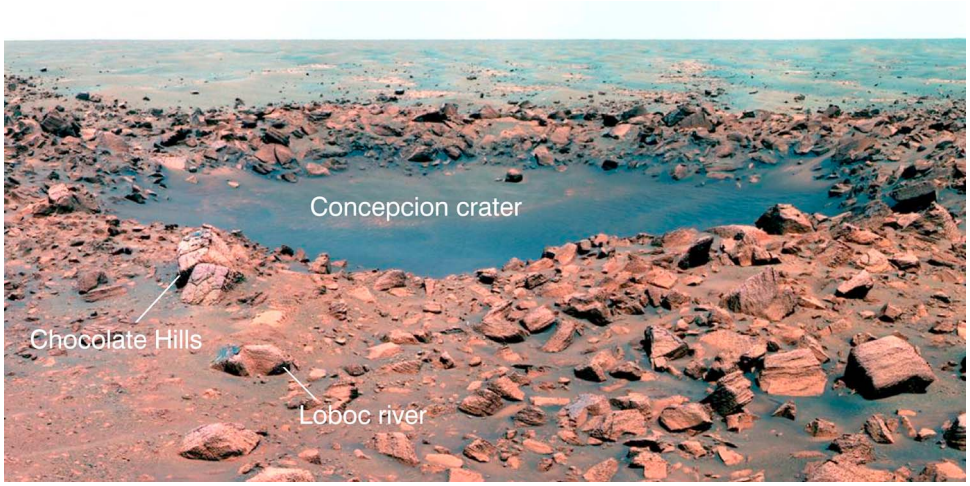

Figure 14. Pancam false color view of Concepción crater acquired on sol 2140, including the Chocolate Hills and Loboc River boulders, when Opportunity was ~5 m from the northern rim. Ejecta from this impact event are superimposed on the surrounding ripples. The crater is partly filled with aeolian basaltic sand. Detailed IDD work was done on Chocolate Hills. Pancam bands L2 (753 nm), L5 (535 nm), and L7 (432 nm) are shown as red, green, and blue colors.

et al., 2010]. The mineralogy and composition of Marquette Island are similar to those of the Adirondack class of basalts examined by Spirit in Gusev crater. It probably originated as an ejecta fragment from an impact event that penetrated the Noachian crust, either beneath the sulfate-rich sedimentary deposits, or from the surrounding Noachian outcrops.

[33] Arkansas is a relatively small, dark cobble that was found close to Erebus crater. It is part of a group of cobbles

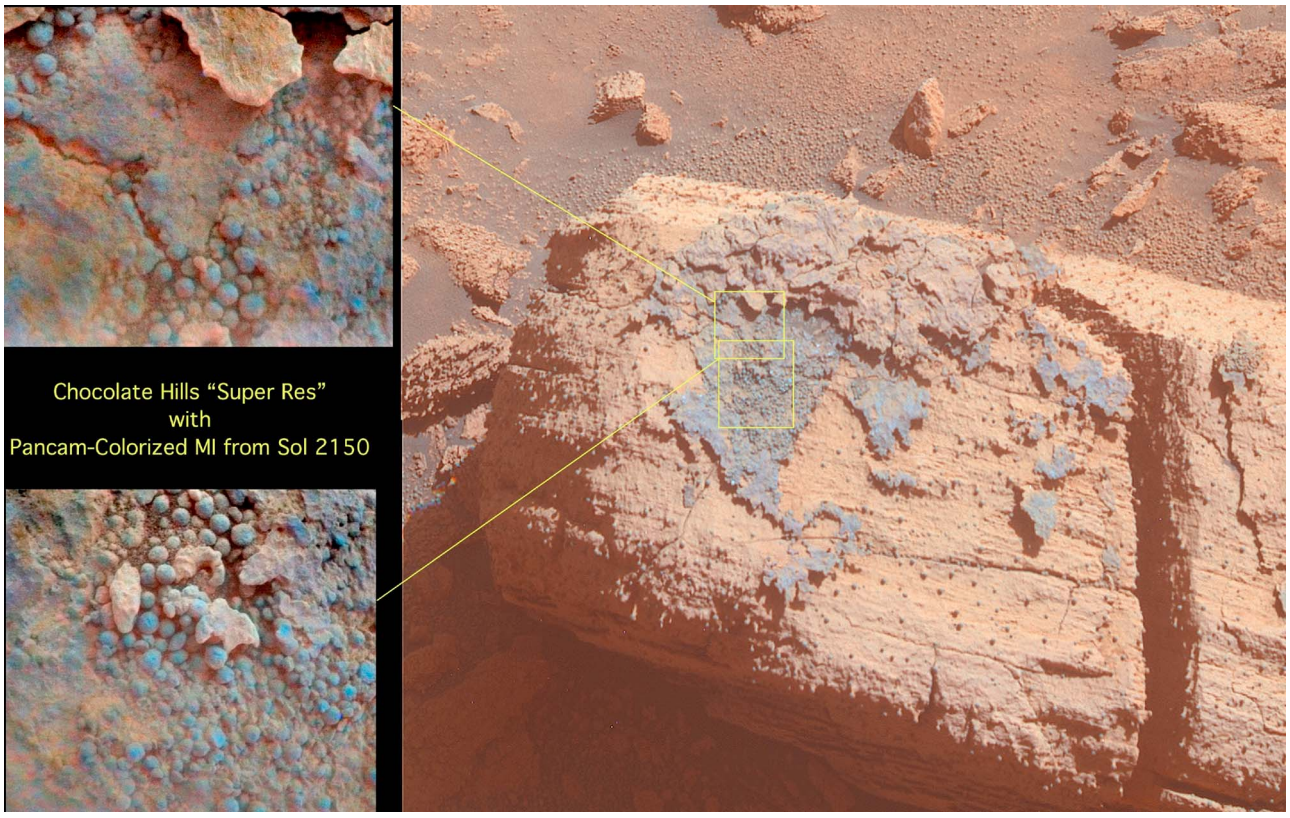

Figure 15. Pancam color view of the Chocolate Hills boulder showing fine-scale layering and a coating of dark material. MI views with Pancam color overlays (labeled "Super Res") show the presence of hematitic concretions. Pancam image acquired on sol 2147 using bands L2 (753 nm), L5 (535 nm), and L7 (432 nm) as red, green, and blue colors, respectively.

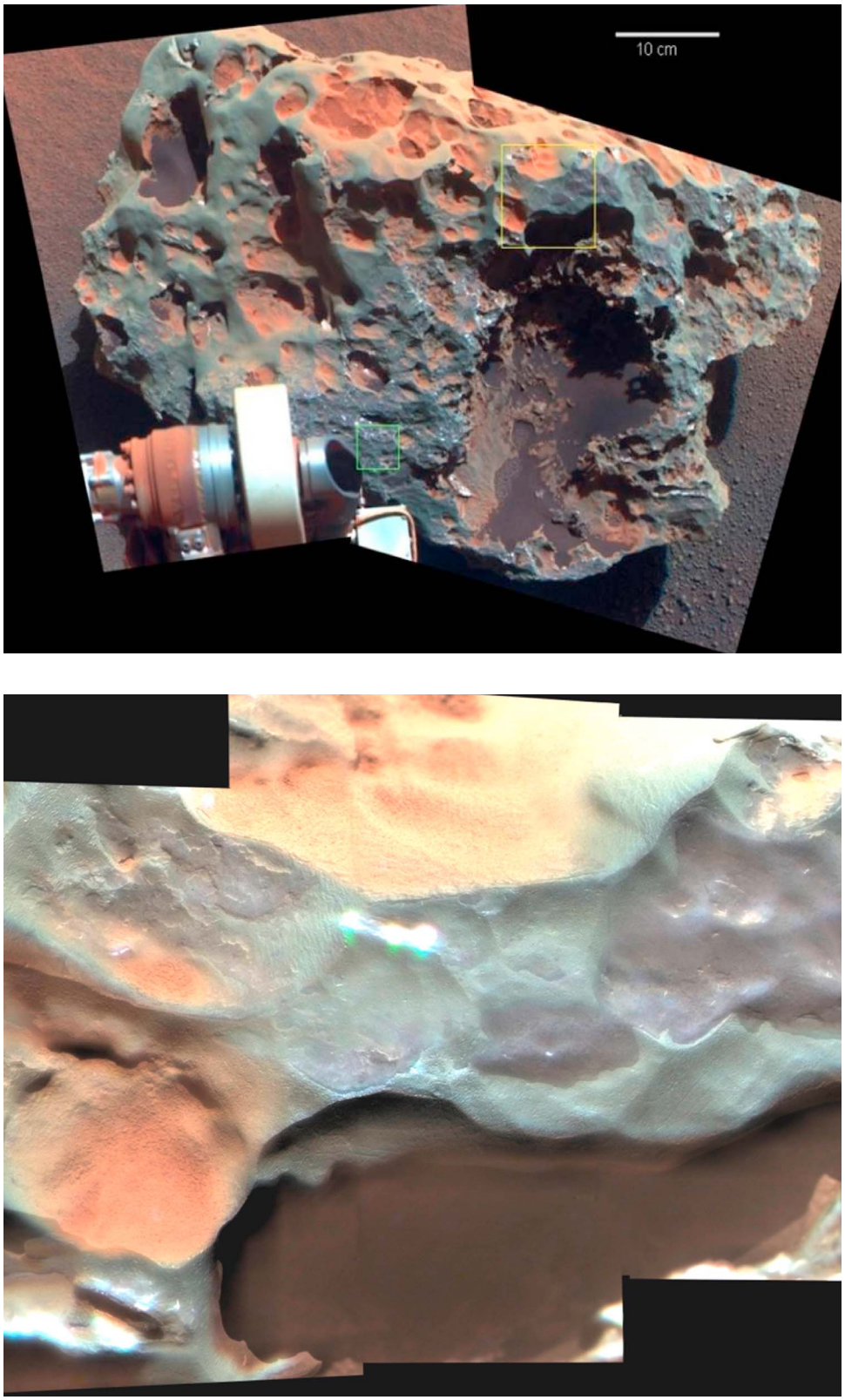

Figure 16. (a) Pancam enhanced false color image (RGB as 753 nm, 535 nm, 432 nm) of the Fe-Ni meteorite Block Island (~65 cm wide). Box outlines areas shown in Figure 16b. (b) MI mosaic of upper portion of Block Island (~7.5 cm across; merged with Pancam false color image) showing purple-hued coatings.

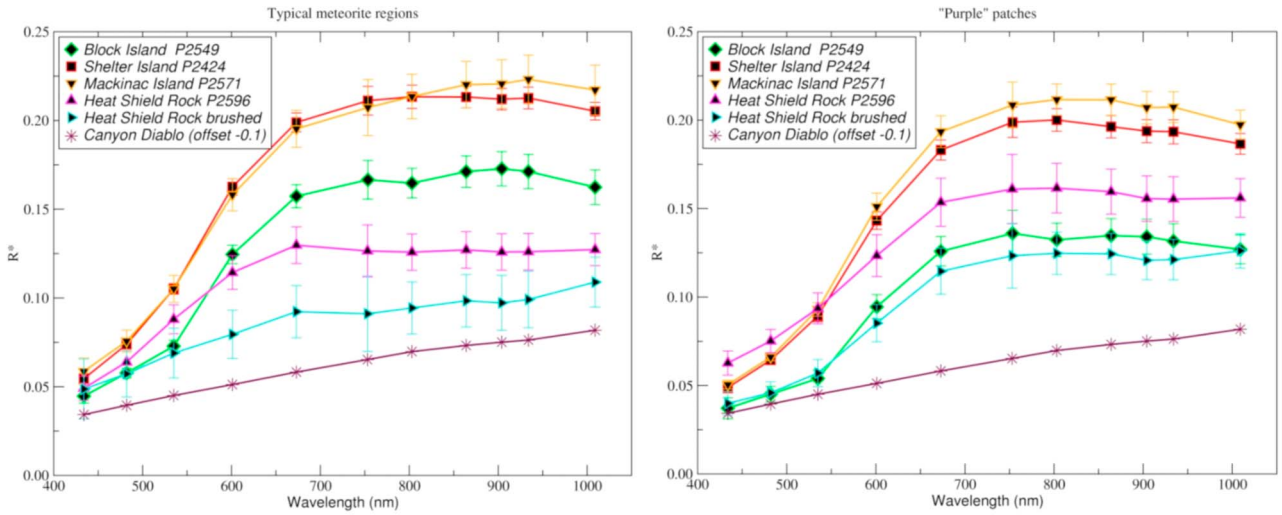

Figure 17. Pancam spectra (R*, relative reflectance normalized to cosine (incidence angle)) of Fe-Ni meteorites for (left) "typical" surfaces and (right) purple surfaces, compared to laboratory spectrum of Canyon Diablo convolved to Pancam band passes (offset by −0.1 for clarity). Spectra for Heat Shield Rock from *Schröder et al.* [2008] show surfaces pristine and brushed using the RAT. Pancam sequence identification numbers shown in legends. Error bars represent standard deviations of pixels selected for regions of interest in Pancam images. Canyon Diablo laboratory spectrum is RELAB MI-CMP-008, spectrum 001.

found during traverses that were too small to brush or grind. Undisturbed surfaces, where large enough to be imaged with the MI, sometimes showed breccia-like textures. The composition and mineralogy of these cobbles indicate a mix of materials, including sulfates. Most likely, the Arkansas group of cobbles represents impact breccias strewn across the surface during local impact events and concentrated on the plains by rapid aeolian erosion of bedrock relative to the more highly indurated cobbles [*Fleischer et al.*, 2010a].

[34] The cobbles of the Barberton group [Barberton (on the southern rim of Endurance), Santa Catarina (part of a strewn field on the rim of Victoria), Santorini, and Kasos] are chemically and mineralogically similar and thus probably have a similar origin [*Schröder et al.*, 2010]. They are similar to mesosiderite meteorite silicate clasts, but may represent a group of meteorites not sampled on Earth. The largest accumulation of Barberton group cobbles, including Santa Catarina, is located near the rim of Victoria crater. It is possible that they are paired fragments of the impactor that formed that crater [*Schröder et al.*, 2008; *Ashley et al.*, 2009; *Schröder et al.*, 2010].

[35] Opportunity has discovered three large (>35 cm) Fe-Ni meteorites (Block Island, Shelter Island, and Mackinac Island) south of Victoria crater [*Fleischer et al.*, 2010b; *Ashley et al.*, 2010]. Each exhibits discontinuous surface coatings that appear purple in Pancam false color images (e.g., Figure 16). For Heat Shield Rock, another Fe-Ni meteorite located to the south of Endurance crater, most RAT-brushed surfaces exhibit Pancam-derived spectra similar to laboratory spectra of the Canyon Diablo IAB meteorite (Figure 17). On the other hand, areas covered with purple coatings exhibit enhanced 535 nm band depths, and more negative spectral slopes between 753 nm and 934 nm, as compared to more typical natural or brushed surfaces on these meteorites (Figure 17). A nanophase iron oxide phase has, in fact, been identified in Mössbauer spectra associated with the purple coatings [*Fleischer et al.*, 2010b]. Additionally, a minor, magnetically ordered iron oxide phase has been identified in spectra from Heat Shield Rock, inferring a small amount of relatively well-crystallized and larger particles (i.e., not nanoparticles) [*Fleischer et al.*, 2010b]. In addition, APXS data for the Fe-Ni meteorites show elevated Br, Zn, and Mg values consistent with surface alteration.

[36] *Schröder et al.* [2008] and *Ashley et al.* [2010] suggested that the coatings on the Fe-Ni meteorites represent remnants of a partially wind-eroded coating that formed when portions of the rock were buried, rather than a remnant fusion crust formed during traverse through the Martian atmosphere. These Fe-Ni meteorites have also undergone significant physical weathering (e.g., Mackinac Island has a cavernous interior) [*Ashley et al.*, 2010]. The length of time that these meteorites have been on or near the surface is difficult to estimate. The size and mass of Heat Shield Rock and Block Island have been used as evidence that they landed during a period when the atmosphere was denser and slowed their descent [*Beech and Coulson*, 2010]. Otherwise they would have been destroyed during the subsequent hypervelocity impact with the surface. Alternatively, the landings would also have been possible with shallow entry angles under current atmospheric conditions [*Chappelow and Golombek*, 2010]. In any case, the extent of weathering of these Fe-Ni meteorites, combined with the presence of iron oxides in the stony-iron meteorites examined by Opportunity, will continue to provide insight into weathering processes on Mars.

[37] Observations of fresh craters younger than the north trending ripples (e.g., the Resolution crater cluster and Concepción) show abundant dark pebbles scattered across their surfaces. Given the apparent young ages of these craters, the straightforward explanation is that these dark pebbles

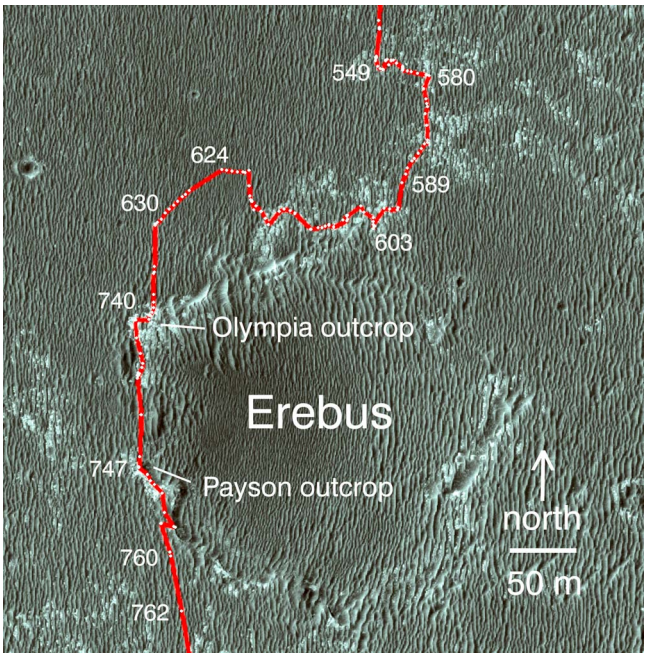

Figure 18. HiRISE view of the highly degraded Erebus crater, with Opportunity traverses shown, along with representative sols and key targets. Opportunity conducted extensive remote sensing and IDD measurements at the Olympia outcrops (bright regions). For the Payson outcrop, which constitutes the southwestern wall of Erebus crater, systematic remote sensing was conducted while Opportunity traversed south toward Victoria crater. Note the extensive north-south trending ripples covering the crater and surrounding plains. Portion of HiRISE frame ESP_016644_1780_red.jp2.

are fragments of the impactors, suggesting that the widespread dark pebbles and cobbles observed by Opportunity at Meridiani Planum are lags of impactor-derived material (either meteoritic or secondary impactors from elsewhere on Mars) [*Golombek et al.*, 2010].

7. Bedrock and Environments of Deposition and Alteration

[38] The sulfate-rich sandstones that comprise the Burns formation and examined by Opportunity within Eagle and Endurance craters provide compelling evidence of deposition by wind, with local subaqueous reworking within interdune ephemeral lakes [e.g., *Squyres et al.*, 2004, 2006; *Grotzinger et al.*, 2005]. Sulfate cements and hematitic concretions attest to multiple, but possibly short-lived episodes of percolation by acidic groundwaters [*McLennan et al.*, 2005]. Recent calculations indicate that in situ iron oxidation could have provided sufficient acidity to explain the Burns formation mineralogy [*Hurowitz et al.*, 2010]. Inferred grain compositions indicate that the sands were sourced in places where waters interacted with and weathered basaltic precursor rocks [*Squyres et al.*, 2004; *Squyres and Knoll*, 2005]. During the period covered by this paper Opportunity explored outcrops on the plains and ventured into Erebus and Victoria craters to continue stratigraphic measurements designed to understand in more detail the origin and environments of deposition that produced the layered sulfate rocks that underlie the Meridiani plains (Figure 1). Particular emphasis was placed on the search for evidence of a sulfate-rich mud facies that might have been the source of the sandstones encountered by Opportunity. Finding those deposits would allow confirmation or rejection of the hypothesis that the sands were sourced in an evaporitic lake environment.

[39] The first set of very detailed measurements focused on the Olympia outcrops exposed to the northwest side of Erebus crater, together with a vertical section, dubbed Payson, on the southwestern wall of Erebus (Figures 18–19). The ripple patterns in these outcrops provide compelling evidence for water transport of sulfate-rich sands, subsequently cemented to become sandstones [*Grotzinger et al.*, 2006; *Metz et al.*, 2009]. The Payson outcrop also showed disruption by water of laminated sandstones and the presence of shrinkage cracks, all consistent with an ephemeral shallow water environment. Compositional and mineralogical measurements acquired at the Olympia outcrops are very similar to measurements acquired in Eagle and Endurance craters. No in situ measurements were acquired at the Payson outcrops. The Olympia area is also the one place where it has proven possible to obtain in situ analyses of fin-like fracture fill, confirming that these features originated as clastic infillings of partings, later cemented to provide differential resistance to erosion. The fill is chemically similar to bedrock materials and not to modern soils. Taken together, the evidence suggests that these features formed after the primary phases of deposition and diagenesis, but prior to deposition of the modern soils [*Knoll et al.*, 2008].

[40] Victoria is the largest crater examined by Opportunity to date, ~750 m wide and ~75 m deep. It was a primary target for exploration during the sols covered by this paper because of the extensive Burns formation stratigraphic exposures on its walls (Figures 2 and 20) [*Squyres et al.*, 2009]. The approach to Victoria from the northwest allowed traversing across the annulus surrounding Victoria, a planar region that was found to consist of aeolian basaltic sands and hematitic concretions that partially cover the tops of beveled ejecta blocks (Figure 21). The ejecta deposit consists of relatively soft sulfate-rich rocks evenly eroded by wind to form the planar annulus that surrounds the crater [*Grant et al.*, 2008]. Remote sensing of the crater wall from various promontories on the rim of Victoria showed that blocky ejecta deposits dominate the upper few meters of wall rock (Figure 22). The ejecta blocks are layered, contain hematitic concretions, and have coloration consistent with an origin as sulfate-rich bedrock. There is no evidence from Victoria's wall rocks or ejecta that the impact event penetrated into the underlying Noachian crust.

[41] Duck Bay was chosen for entry into Victoria for detailed measurements because of the extensive Burns formation outcrops and the relatively easy ingress and exit paths (Figure 23). Beneath the ejecta deposit exposed at Duck Bay are four discrete layers that were examined using both remote sensing and in situ instrumentation [*Squyres et al.*, 2009]. Steno is the layer in contact with the ejecta and is underlain by a relatively bright layer, Smith. Lyell and Gilbert are the next two layers examined during the Duck Bay campaign. Steno consists of a fine to medium-grained

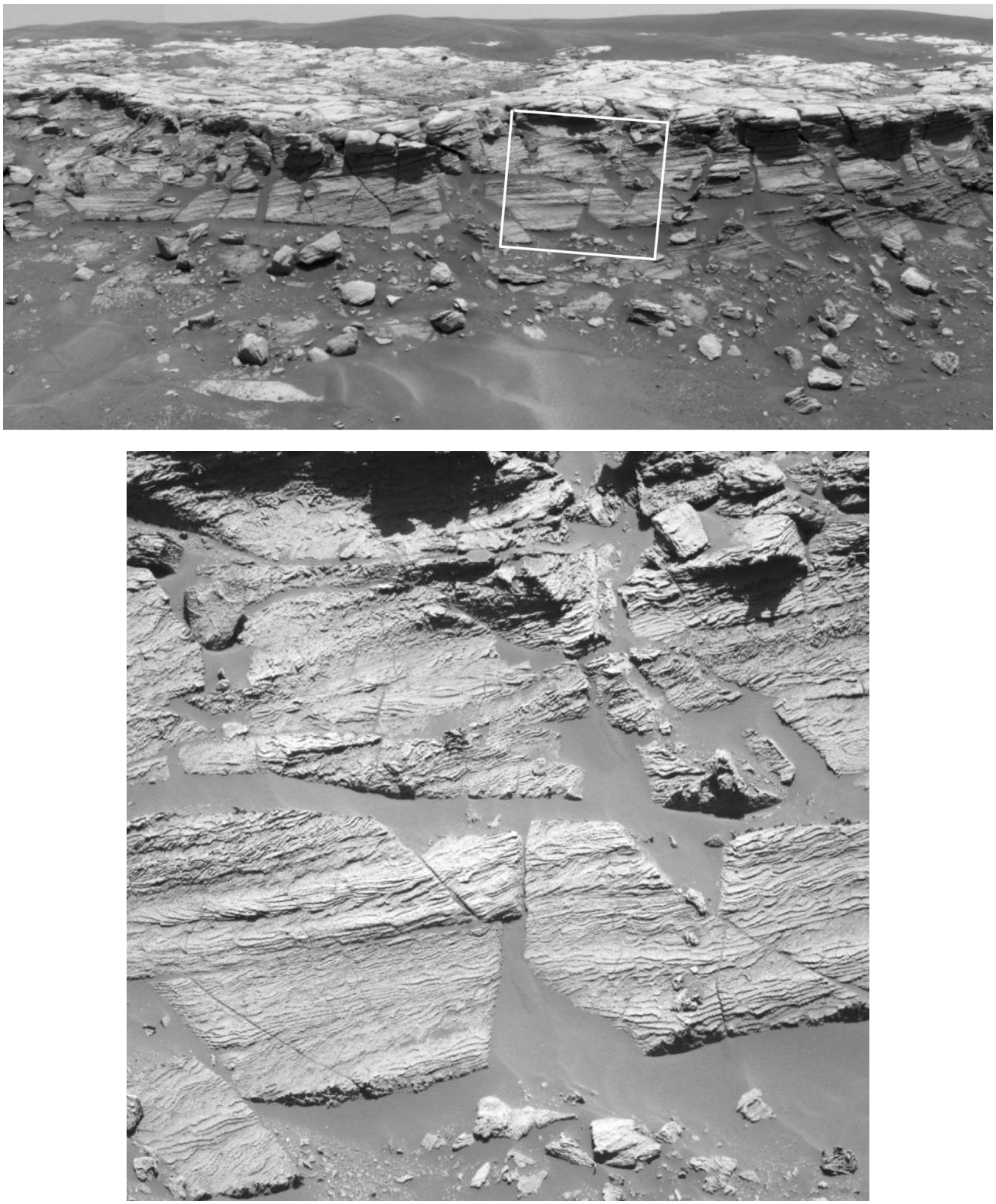

Figure 19. (a) Portion of a Navcam mosaic looking toward the west of a portion of the Payson outcrop acquired on sol 747. The outcrop height is ~1.6 m and relatively dark ripples are shown in the plains beyond Payson. Note the outcrop cross bedding dipping toward the south. Box shows location of Pancam frame shown in Figure 19b. (b) Pancam view of a portion of the Payson outcrop showing approximately a dozen fine-scale, cross-bedded layers. The ripple patterns are indicative of shallow subaqueous transport, similar in interpretation to the ripple patterns in the sandstones observed to the north in the Olympia outcrop on the northwestern side of Erebus. Height covered in the image is ~1.4 m. Pancam frame 1P194853277RSD646BP2547L7MZ acquired on sol 751.

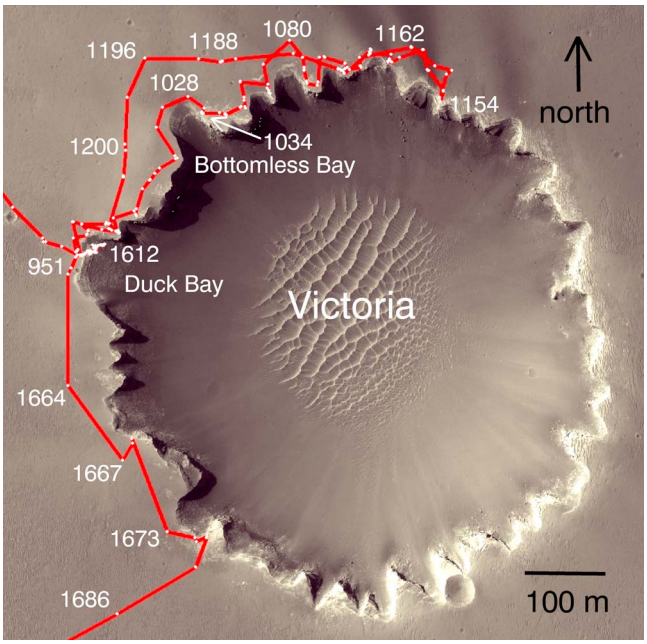

Figure 20. HiRISE view of Victoria crater showing Opportunity's traverses, including drives into and out of Duck Bay for detailed IDD work on outcrops. The outcrop examined by Opportunity within Bottomless Bay is shown in a Pancam color view in Figure 22a. Traverses around a portion of Victoria's rim were conducted to map outcrops and to find a bay into which ingress and exit could be made with relatively low risk of embedding. Portion of HiRISE frame ESP_016644_1780_red.jp2.

sandstone with well-defined laminae. Cross bedding is evident, as are hematitic concretions. Steno is separated from Smith by an unconformity. Smith is a relatively bright sandstone and exhibits fine-scale laminations. Lyell is transitional with Smith and exhibits tabular, prismatic vugs, cross bedding, and an abundance of hematitic concretions. Gilbert was only measured in one location and the contact with Lyell is gradational. Lyell and Smith are also sandstones. Pancam observations show that the Smith unit has an abrupt spectral downturn at 1000 nm, consistent with the presence of the molecular water vibrational mode 2v1 + v3 and 3vOH for OH-bearing minerals (Figure 23) [see *Rice et al.*, 2011]. No evidence was found in any of the layers for the mud facies that might have been the source for the sulfate-rich sandstones. In fact, the rocks examined in Victoria, both using remote sensing from capes, and detailed measurements in Duck Bay, are best interpreted as sulfate-rich aeolian sands altered and cemented by groundwater infiltration [*Squyres et al.*, 2009].

[42] In situ data were acquired for undisturbed, brushed, and ratted rock targets within each of the four stratigraphic layers in Duck Bay. Correspondence analysis shows the importance of removing aeolian sand and dust covers and any coatings from these rocks to understand their intrinsic characteristics (Figure 24). In particular, the first factor in APXS data, accounting for 92% of the variance of the data set, shows a trend from basaltic to more sulfate-rich materials for natural, brushed, as opposed to ratted targets. Ratted targets have the highest sulfur content and least contamination by coatings or basaltic sands. The second factor, accounting for 4% of the variance, shows that the ratted rock targets can be discriminated from one another on the basis of chlorine content, with Gilbert showing the highest value, and Steno the lowest. A trend of increasing chlorine content with increasing depth is also evident in a scatterplot of chlorine to silica content as a function of depth (Figure 25). On the other hand, the sulfur and magnesium contents, relative to silica, both decrease as a function of depth beneath the surface (Figure 26). These compositional patterns correlate well with the hydration index computed from the depth of the 1000 nm band evident in the Smith unit (Figure 24). Further, this bright, upper unit appears to continue around the entire crater and can be fit with a horizontal plane (A. Hayes et al., Reconstruction of eolian bedforms and paleocurrents from cross-bedded strata at Victoria crater, Meridiani Planum, Mars, submitted to *Journal of Geophysical Research*, 2011).

[43] The rocks examined in Duck Bay, although still part of the Burns formation, are separated laterally and topographically from the Karatepe section outcrops examined in Endurance crater. Even so, the Karatepe section also shows a bright upper layer (above the Whatanga contact) that is depleted in chlorine relative to silica and enhanced in magnesium and sulfur relative to silica as compared to rocks exposed at greater depths (Figures 25–26) [see also *Squyres et al.*, 2009]. In addition, the VNIR multispectral character of both sets of strata is similar [*Farrand et al.*, 2007]. A. Hayes et al. (submitted manuscript, 2011), examining orbital data, found that bright layers are evident in a number of other craters that formed in the Burns formation. Overall, the evidence is interpreted to reflect regional-scale differential vertical mobility of soluble sulfate and chloride salts during near surface aqueous-mediated diagenesis [*Clark et al.*, 2005; *Amundson et al.*, 2008]. The observation that Victoria ejecta deposits include fragments of the Smith unit implies that the aqueous alteration event predates formation of Victoria [*Edgar et al.*, 2010].

8. Rim of Endeavour Crater and Adjacent Layered Sedimentary Rocks

[44] Opportunity has thus far been exploring sedimentary rocks and soils that unconformably overlie the Noachian crust (Figure 1). Endeavour crater predates the sedimentary deposits and the crater rim exposes materials of Noachian age (Figures 1, 27, and 28). This is clear from geologic mapping and also initial spectral analysis of CRISM hyperspectral data [*Murchie et al.*, 2007] covering the rim and surrounding areas. Specifically, *Wray et al.* [2009] showed from analysis of CRISM spectra covering 0.4 to 2.5 μm in wavelength that portions of the rim expose iron and magnesium-rich smectite clay minerals. In addition, these authors showed that the sedimentary rocks adjacent to the rim have spectra that are indicative of hydrated sulfates.

[45] The long-term objectives for the Opportunity extended mission are to drive to the hydrated sulfate deposits and Noachian-aged rim materials of Endeavour. By sol 2239 the rover was within ~11 km of the rim (Figure 27). Pancam color and superresolution imaging (Figure 28), combined with periodic collection of imaging data from the HiRISE, CTX, and CRISM instruments, are helping to

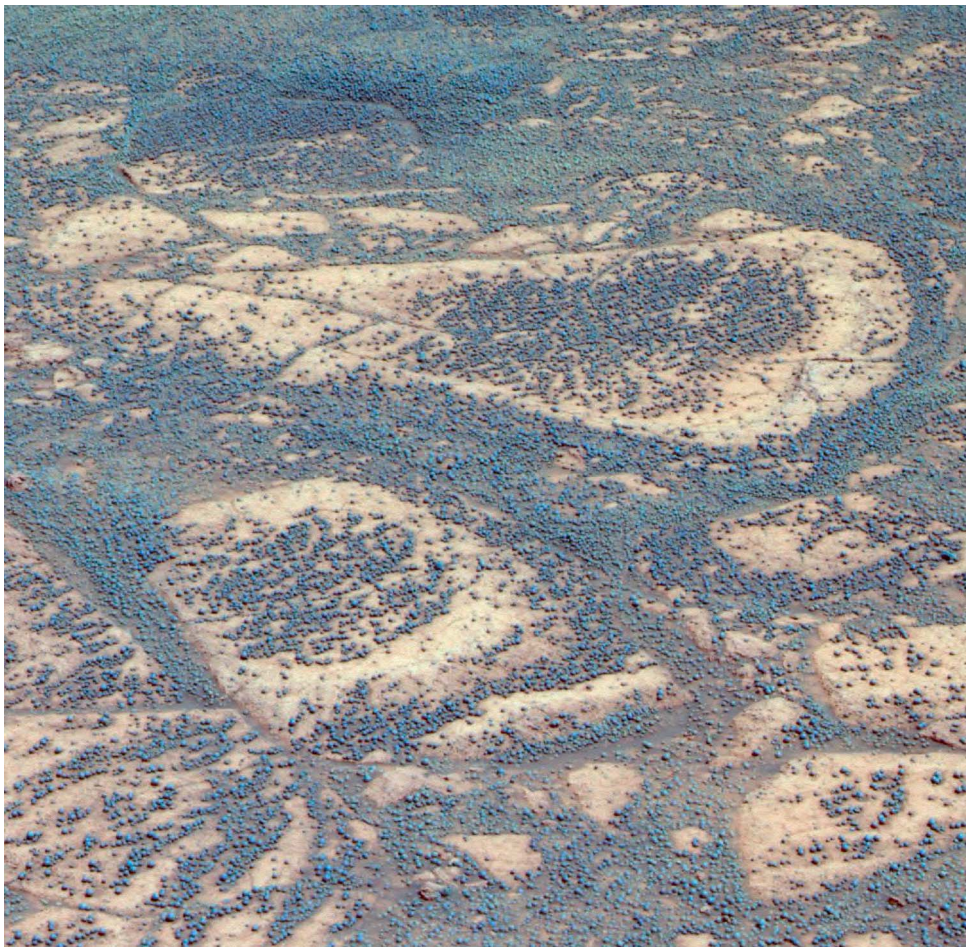

Figure 21. Pancam false color view of the Victoria ejecta deposit apron showing the tops of boulders that have been leveled by aeolian erosion and partially covered by soil with a relatively high concentration of hematitc concretions. The tear drop–shaped boulder on the top half of the frame is ~0.9 m long. The target area is Malua, and the data were acquired on sol 1029. Pancam bands L2 (753 nm), L5 (535 nm), and L6 (482 nm) are shown as red, green, and blue colors.

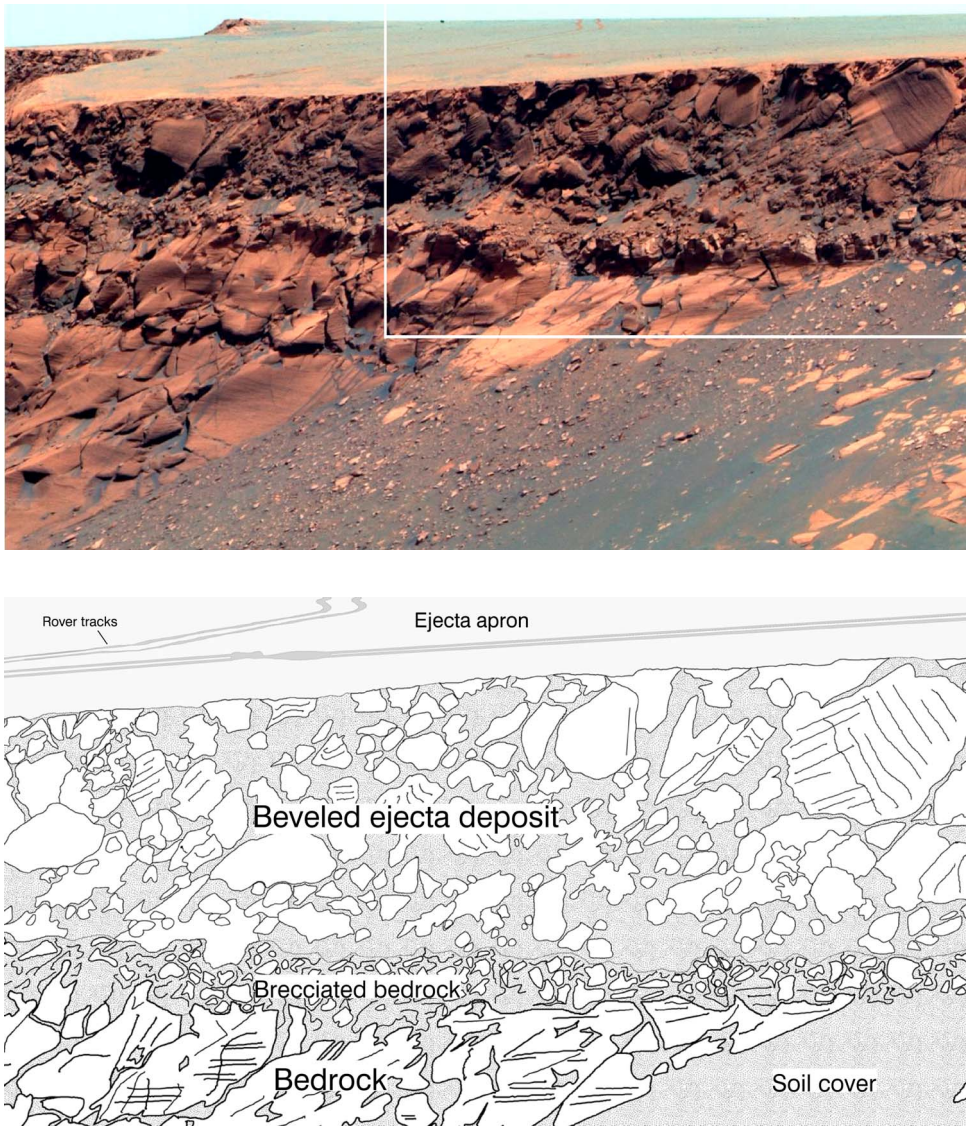

Figure 22. (a) Pancam false color view of the outcrop on the southwestern side of Bottomless Bay and a portion of the overlying ejecta deposit and annulus. Box shows region for which a geologic sketch map is shown in Figure 22b. Data acquired on sol 1037. Pancam bands 2 (0.753 μm), 5 (0.535 μm), and 7 (0.432 μm) are shown as red, green, and blue colors. (b) Geologic sketch map showing in-place bedrock, fractured bedrock, and poorly sorted ejecta blocks superimposed on the fracture bedrock surface. The ejecta has been leveled by aeolian erosion to form the annulus surrounding Victoria. Note rover tracks.

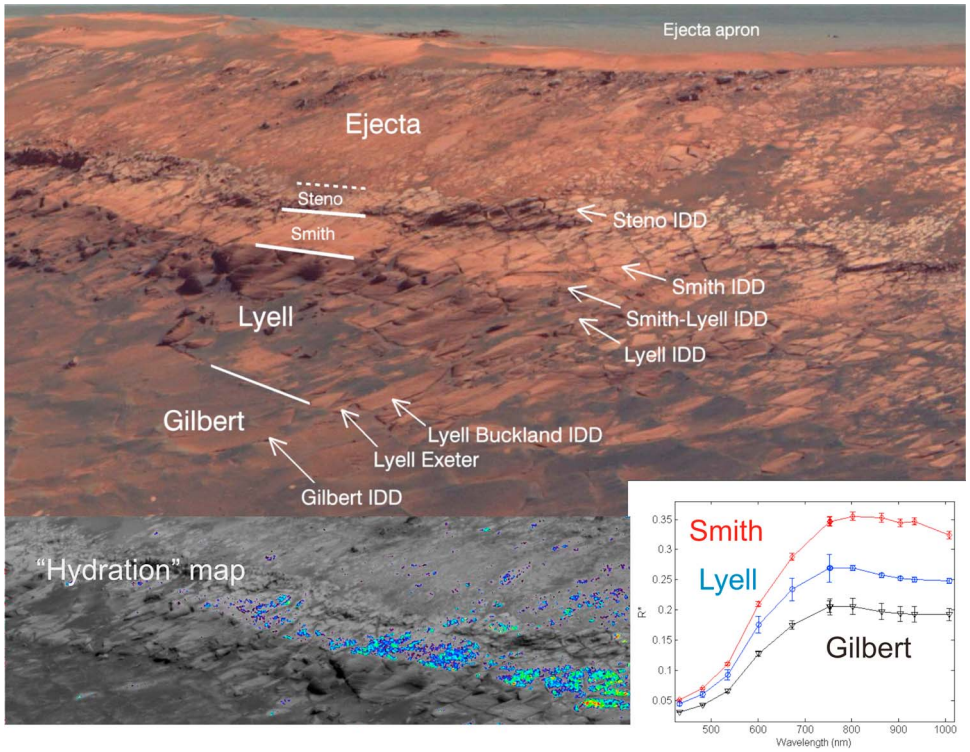

Figure 23. Portion of a Pancam false color mosaic covering the stratigraphic section examined by Opportunity during its traverses within Duck Bay, Victoria crater. The mosaic data were acquired between sols 970 to 991 as part of the Cape Verde panorama. Steno is the topmost in-place outcrop beneath the ejecta deposit. The brighter layer, Smith, can be found in many locations around the perimeter of the crater. Pancam 13F spectra for Smith, Lyell, and Gilbert are shown in the lower right and discussed in detail in the text. A hydration index based in the depth of the 1.0 μm band is shown on the lower left and indicates that the Smith unit is hydrated. The hydration index covers the left portion of the Pancam false color mosaic and is centered vertically on the Smith unit. Pancam bands 2 (753 nm), 5 (535 nm), and 7 (432 nm) are shown as red, green, and blue colors.

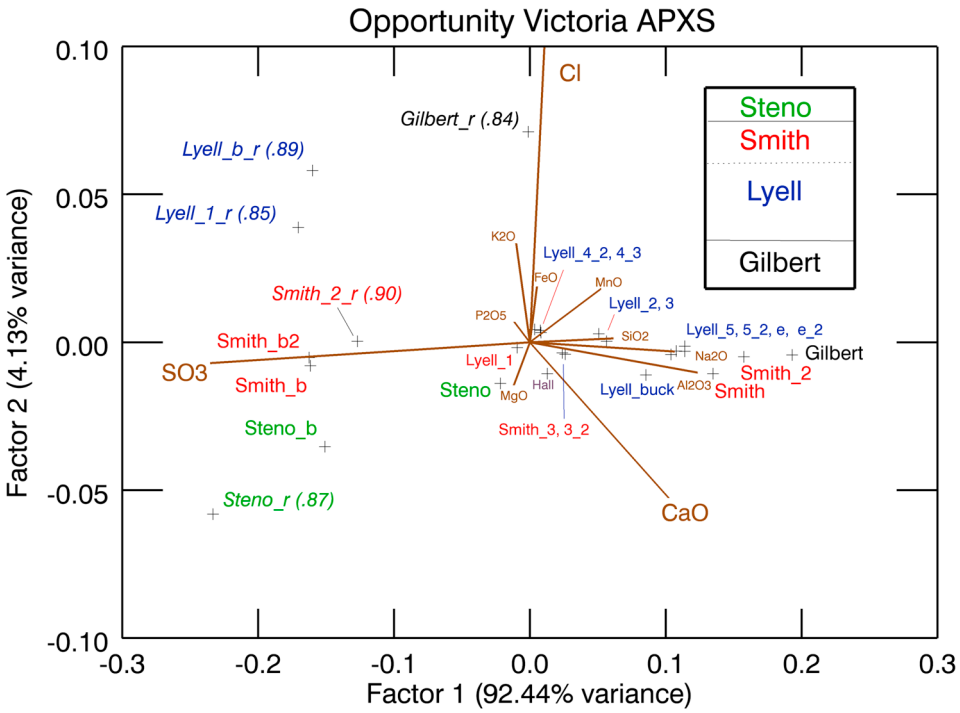

Figure 24. Correspondence analysis plot for APXS data acquired for rock outcrops in Duck Bay, Victoria crater. The highest fractional variance is controlled by changes in chemistry from natural surfaces, contaminated by aeolian basaltic soils and coatings, to ratted surfaces that better represent the sulfate-rich outcrop chemistry. Brushed targets are denoted by "_b" after names. Targets in italics have been ratted ("_r"), and numbers in parentheses correspond to ferric iron to total iron values from MB observations. The direction of second highest fractional variance separates ratted targets based on chlorine, sulfur, and magnesium contents, as shown by scatterplots in Figures 25 and 26. Box in the top right corner is a schematic stratigraphic section.

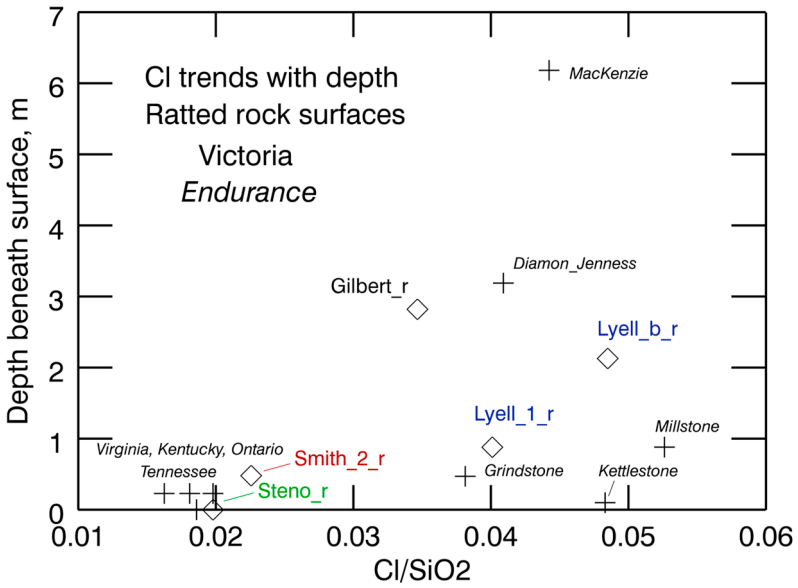

Figure 25. APXS-based chlorine/SiO_2 values are shown as a function of depth beneath the ejecta to bedrock contact for ratted targets in Victoria and Endurance craters. The presence of the bright upper layer in both craters and the increase in Cl/SiO_2 with increasing depth indicates a regional-scale aqueous process that concentrated relatively soluble Cl in lower stratigraphic horizons. The bright layer corresponds to the Smith unit in Victoria and to rock targets above the Whatanga contact for the Endurance Karatepe section. Endurance targets Virginia, Kentucky, Ontario, and Tennessee are above the Whatanga contact.

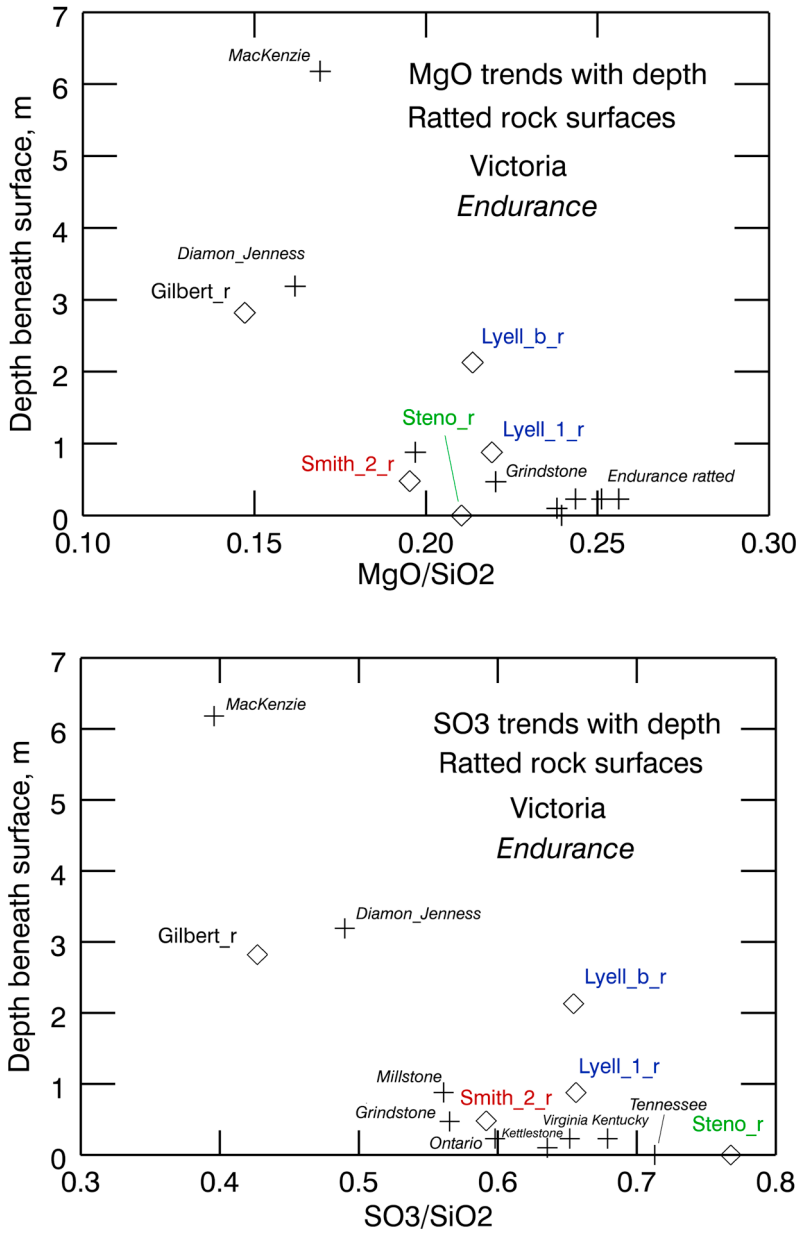

Figure 26. Decreasing values of (top) MgO and (bottom) SO_3 relative to SiO_2 with depth beneath the ejecta to bedrock contact for both Endurance and Victoria craters, implying a regional-scale aqueous alteration process that led to an enrichment of relatively insoluble magnesium sulfates in the bedrock upper layers.

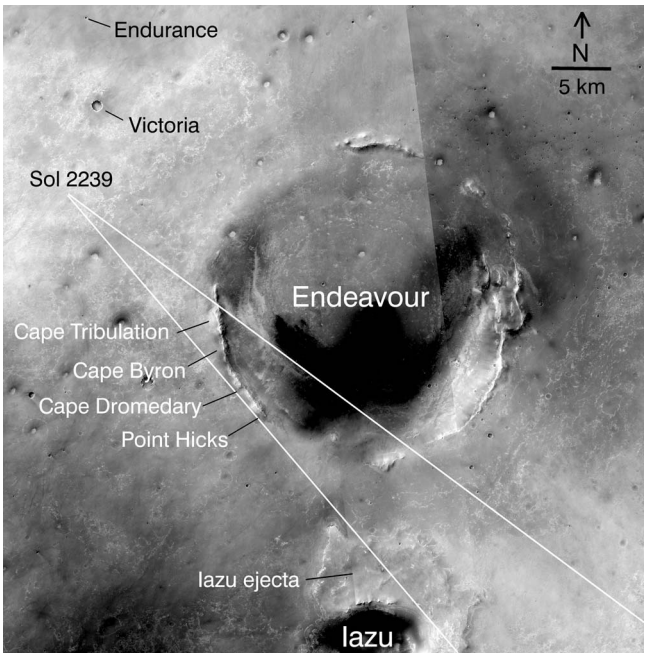

Figure 27. CTX mosaic with Opportunity traverses shown and locations on the rim of Endeavour labeled. The white lines extending from the sol 2239 position cover the field of view of the Pancam superresolution images of the rim of Endeavour shown in Figure 28. Mosaic generated from CTX frames P13_006135_1789_XN_01S005W_071117, P15_006847_1770_XN_03S005W_080111, and P17_007849_1793_XN_00S005W_080330.

define traverses to locations where the hydrated sulfate sedimentary rocks and altered rim materials are best exposed and accessible to Opportunity. Outcrops of the Burns formation that have been characterized thus far by Opportunity exhibit OMEGA-based and CRISM-based reflectance spectra that indicate the spectral dominance of relatively anhydrous phases [e.g., *Arvidson et al.*, 2006]. This result is consistent with the dominance of nanophase iron oxide coatings on rock surfaces [e.g., *Knoll et al.*, 2008], and with the observation that the 6 μm bending vibration for water is not evident in Mini-TES for undisturbed rock surfaces [*Glotch et al.*, 2006]. On the other hand, Mini-TES deconvolution of ratted Burns formation material, including constraints from MB and APXS measurements, indicate the presence of hydrated Mg and Ca-sulfate minerals [*Glotch et al.*, 2006]. The surface exposures of hydrated sulfates close to the rim of Endeavour are likely layers that lie stratigraphically beneath the Burns formation rocks examined by Opportunity. Characterizing the composition, mineralogy, and texture of these older sedimentary rocks will provide new information on paleoenvironmental conditions and perhaps even provide the evidence for the source rocks for the sulfate-rich aeolian sandstones that dominate the Burns formation. In addition, Opportunity's characterization of Endeavour's rim rocks, including clay minerals, will allow even older environmental conditions to be reconstructed.

9. Conclusions

[46] Opportunity has been traversing across the plains of Meridiani since January 2004, far exceeding the expected lifetimes and traverse distances of the rover, and using its Athena scientific payload for many more measurements than originally planned. Opportunity has operated over three Martian years and acquired important information on modern atmospheric dynamics, including atmospheric opacity, clouds, and use of atmospheric argon as a tracer for circulation dynamics. The aeolian ripples traversed by Opportunity were generated by easterly winds in an ancient environment, probably within hundreds of thousands of years, when the spin axis obliquity was higher and Hadley cell circulation enhanced. Cobbles and boulders examined by Opportunity include local and regional-scale ejecta blocks, together with both stony iron and iron-nickel meteorites. The meteorites have undergone both physical and chemical weathering and are likely a lag of impactor-derived materials. Opportunity has made measurements within Eagle, Endurance, Erebus, and Victoria craters, together with outcrop exposures on the plains that were focused on characterizing the formation and modification of the Burns formation sulfate-rich sandstones. Results continue to show compelling evidence of sand deposition by wind, with local reworking within ephemeral lakes. Extensive

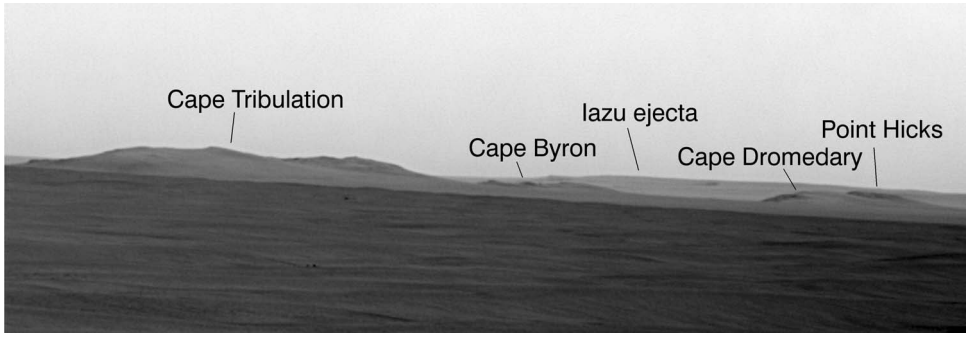

Figure 28. Pancam superresolution view of a portion of Endeavour's rim and Iazu ejecta acquired from ~13 km distance. Cape Tribulation has exposures of Fe-Mg smectite clay minerals based on analyses of CRISM data [*Wray et al.*, 2009]. Analysis of CRISM data also indicate the presence of layered sedimentary rocks with hydrated sulfate signatures adjacent to the rim [*Wray et al.*, 2009]. This image was generated from a series of eight Pancam frames acquired on sol 2239.

lacustrine evaporitic facies have not yet been found, although particular emphasis has been placed on finding these putative materials. Accessing the hydrated sulfate rocks near the Endeavour crater rim and the clay minerals on the rim proper will open a new chapter for Opportunity and allow characterization of materials not yet encountered during the mission.

[47] **Acknowledgments.** We thank the capable team of engineers and scientists at the Jet Propulsion Laboratory and elsewhere who made the Opportunity mission possible. We also thank support from NASA for the MER science team to allow both collection and analysis of data from Opportunity. Alejandro Soto and Mark Richardson provided valuable comments on an earlier draft of this paper and we thank them for their efforts. Thanks to Emma Reinemann for helping with several figures.

References

Amundson, R., S. Ewing, W. Dietrich, B. Sutter, J. Owen, O. Chadwick, K. Nishiizumi, M. Walvoord, and C. McKay (2008), On the in situ aqueous alteration of soils on Mars, *Geochim. Cosmochim. Acta*, *72*, 3845–3864, doi:10.1016/j.gca.2008.04.038.

Andrews-Hanna, J. C., M. T. Zuber, R. E. Arvidson, and S. J. Wiseman (2010), Early Mars hydrology: Meridiani playa deposits and the sedimentary record of Arabia Terra, *J. Geophys. Res.*, *115*, E06002, doi:10.1029/2009JE003485.

Arvidson, R. E., et al. (2006), Nature and origin of the hematite-bearing plains of Terra Meridiani based on analysis of orbital and Mars Exploration Rover data sets, *J. Geophys. Res.*, *111*, E12S08, doi:10.1029/2006JE002728.

Arvidson, R. E., et al. (2008), Spirit Mars Rover Mission to the Columbia Hills, Gusev crater: Mission overview and selected results from the Cumberland Ridge to Home Plate, *J. Geophys. Res.*, *113*, E12S33, doi:10.1029/2008JE003183.

Arvidson, R. E., et al. (2010), Spirit Mars Rover Mission: Overview and selected results from the northern Home Plate Winter Haven to the side of Scamander crater, *J. Geophys. Res.*, *115*, E00F03, doi:10.1029/2010JE003633.

Ashley, J. W., S. W. Ruff, A. T. Knudson, and P. R. Christensen (2009), Mini-TES measurements of Santa Catarina-type, stony-iron meteorite candidates by the Opportunity rover, *Lunar Planet. Sci.*, *XL*, Abstract 2468.

Ashley, J. W., M. P. Golombek, P. R. Christensen, I. Fleischer, K. E. Herkenhoff, J. R. Johnson, T. J. McCoy, T. J. Parker, C. Schröder, and S. W. Squyres (2010), Evidence for mechanical and chemical alteration of three new iron-nickel meteorites on Mars: Process insights for Meridiani Planum, *J. Geophys. Res.*, doi:10.1029/2010JE003672, in press.

Beech, M., and I. M. Coulson (2010), The making of Martian meteorite Block Island, *Mon. Not. R. Astron. Soc.*, *404*, 1457–1463, doi:10.1111/j.1365-2966.2010.16350.x.

Chappelow, J., and M. Golombek (2010), Entry and landing conditions that produced Block Island, *J. Geophys. Res.*, *115*, E00F07, doi:10.1029/2010JE003666.

Christensen, P. R., R. V. Morris, M. D. Lane, J. L. Bandfield, and M. C. Malin (2001), Global mapping of Martian hematite mineral deposits: Remnants of water-driven processes on early Mars, *J. Geophys. Res.*, *106*(E10), 23,873–23,885, doi:10.1029/2000JE001415.

Christensen, P. R., et al. (2004a), The Thermal Emission Imaging System (THEMIS) for the Mars 2001 Odyssey mission, *Space Sci. Rev.*, *110*, 85–130, doi:10.1023/B:SPAC.0000021008.16305.94.

Christensen, P. R., et al. (2004b), Mineralogy at Meridiani Planum from the Mini-TES Experiment on the Opportunity rover, *Science*, *306*, 1733–1739, doi:10.1126/science.1104909.

Clancy, R. T., A. W. Grossman, M. J. Wolff, P. B. James, D. J. Rudy, Y. N. Billawala, B. J. Sandor, S. W. Lee, and D. O. Muhleman (1996), Water vapor saturation at low altitudes around Mars aphelion: A key to Mars climate?, *Icarus*, *122*, 36–62, doi:10.1006/icar.1996.0108.

Clark, B. C., et al. (2005), Chemistry and mineralogy of outcrops at Meridiani Planum, *Earth Planet. Sci. Lett.*, *240*, 73–94, doi:10.1016/j.epsl.2005.09.040.

Connolly, H. C., et al. (2006), Meteoritical bulletin #90, *Meteorit. Planet. Sci.*, *41*(9), 1383–1418, doi:10.1111/j.1945-5100.2006.tb00529.x.

Edgar, L., J. Grotzinger, A. Hayes, D. Rubin, J. Bell, and S. W. Squyres (2010, submitted), Stratigraphic architecture of bedrock outcrops, Victoria crater, Meridiani Planum, Mars, in *SEPM Special Publication: Martian Environmental History and Sedimentary Processes*, edited by J. Grotzinger and R. Milliken.

Farrand, W. H., et al. (2007), Visible and near-infrared multispectral analysis of rocks at Meridiani Planum, Mars, by the Mars Exploration Rover Opportunity, *J. Geophys. Res.*, *112*, E06S02, doi:10.1029/2006JE002773.

Fenton, L. K., and M. I. Richardson (2001), Martian surface winds: Insensitivity to orbital changes and implications for aeolian processes, *J. Geophys. Res.*, *106*(E12), 32,885–32,902, doi:10.1029/2000JE001407.

Fergason, R. L., P. R. Christensen, and H. H. Kieffer (2006), High-resolution thermal inertia derived from the Thermal Emission Imaging System (THEMIS): Thermal model and applications, *J. Geophys. Res.*, *111*, E12004, doi:10.1029/2006JE002735.

Fleischer, I., et al. (2010a), Mineralogy and chemistry of cobbles at Meridiani Planum, Mars, investigated by the Mars Exploration Rover Opportunity, *J. Geophys. Res.*, *115*, E00F05, doi:10.1029/2010JE003621.

Fleischer, I., G. Klingelhöfer, C. Schröder, D. W. Mittlefehldt, R. V. Morris, M. Golombek, and J. W. Ashley (2010b), In situ investigation of iron meteorites at Meridiani Planum, Mars, *Lunar Planet. Sci.*, *XLI*, Abstract 1791.

Geissler, P. E., R. Sullivan, M. Golombek, J. R. Johnson, K. Herkenhoff, N. Bridges, A. Vaughan, J. Maki, T. Parker, and J. Bell (2010), Gone with the wind: Eolian erasure of the Mars rover tracks, *J. Geophys. Res.*, *115*, E00F11, doi:10.1029/2010JE003674.

Glotch, T. D., J. L. Bandfield, P. R. Christensen, W. M. Calvin, S. M. McLennan, B. C. Clark, A. D. Rogers, and S. W. Squyres (2006), Mineralogy of the light-toned outcrop rock at Meridiani Planum as seen by the Miniature Thermal Emission Spectrometer and implications for its formation, *J. Geophys. Res.*, *111*, E12S03, doi:10.1029/2005JE002672.

Golombek, M., K. Robinson, A. McEwen, N. Bridges, B. Ivanov, L. Tornabene, and R. Sullivan (2010), Constraints on ripple migration at Meridiani Planum from Opportunity and HiRISE observations of fresh craters, *J. Geophys. Res.*, *115*, E00F08, doi:10.1029/2010JE003628.

Grant, J. A., S. A. Wilson, B. A. Cohen, M. P. Golombek, P. E. Geissler, R. J. Sullivan, R. L. Kirk, and T. J. Parker (2008), Degradation of Victoria crater, Mars, *J. Geophys. Res.*, *113*, E11010, doi:10.1029/2008JE003155.

Grotzinger, J. P., et al. (2005), Stratigraphy and sedimentology of a dry to wet eolian depositional system, Burns formation, Meridiani Planum, Mars, *Earth Planet. Sci. Lett.*, *240*, 11–72, doi:10.1016/j.epsl.2005.09.039.

Grotzinger, J. P., et al. (2006), Sedimentary textures formed by aqueous processes, Erebus crater, Meridiani Planum, Mars, *Geology*, *34*, 1085–1088, doi:10.1130/G22985A.1.

Haberle, R. M., J. R. Murphy, and J. Schaeffer (2003), Orbital change experiments with a Mars general circulation model, *Icarus*, *161*, 66–89, doi:10.1016/S0019-1035(02)00017-9.

Hurowitz, J. A., W. W. Fischer, N. J. Tosca, and R. E. Milliken (2010), Origin of acidic surface waters and the evolution of atmospheric chemistry on early Mars, *Nat. Geosci.*, *3*, 323–326, doi:10.1038/ngeo831.

Jerolmack, D. J., D. Mohrig, J. P. Grotzinger, D. A. Fike, and W. A. Watters (2006), Spatial grain size sorting in eolian ripples and estimation of wind conditions on planetary surfaces: Application to Meridiani Planum, Mars, *J. Geophys. Res.*, *111*, E12S02, doi:10.1029/2005JE002544.

Knoll, A. H., et al. (2008), Veneers, rinds, and fracture fills: Relatively late alteration of sedimentary rocks at Meridiani Planum, Mars, *J. Geophys. Res.*, *113*, E06S16, doi:10.1029/2007JE002949.

Maimone, M., Y. Cheng, and L. Matthies (2007), Two years of visual odometry on the Mars Exploration Rovers, *J. Field Robot.*, *24*(3), 169–186, doi:10.1002/rob.20184.

Malin, M. C., et al. (2007), Context Camera Investigation on board the Mars Reconnaissance Orbiter, *J. Geophys. Res.*, *112*, E05S04, doi:10.1029/2006JE002808.

McEwen, A. S., et al. (2007), Mars Reconnaissance Orbiter's High Resolution Imaging Science Experiment (HiRISE), *J. Geophys. Res.*, *112*, E05S02, doi:10.1029/2005JE002605.

McLennan, S. M., et al. (2005), Provenance and diagenesis of sedimentary rocks in the vicinity of the Opportunity landing site, Meridiani Planum, Mars, *Earth Planet. Sci. Lett.*, *240*, 95–121, doi:10.1016/j.epsl.2005.09.041.

Metz, J. M., J. P. Grotzinger, D. M. Rubin, K. W. Lewis, S. W. Squyres, and J. F. Bell (2009), Sulfate-rich eolian and wet interdune deposits, Erebus crater, Meridiani Planum, Mars, *J. Sediment. Res.*, *79*, 247–264, doi:10.2110/jsr.2009.033.

Mittlefehldt, D. W., et al. (2010), Marquette Island: A distinct mafic lithology discovered by Opportunity, *Lunar Planet. Sci.*, *XLI*, Abstract 1533.

Morris, R. V., et al. (2010), Identification of carbonate-rich outcrops on Mars by the Spirit rover, *Science*, *329*, 421–424, doi:10.1126/science.1189667.

Murchie, S. L., et al. (2007), Compact Reconnaissance Imaging Spectrometer for Mars (CRISM) on Mars Reconnaissance Orbiter (MRO), *J. Geophys. Res.*, *112*, E05S03, doi:10.1029/2006JE002682.

Nelli, S. M., J. R. Murphy, A. L. Sprague, W. V. Boynton, K. E. Kerry, D. M. Janes, and A. E. Metzger (2007), Dissecting the polar dichotomy of the noncondensable gas enhancement on Mars using the NASA Ames Mars General Circulation Model, *J. Geophys. Res.*, *112*, E08S91, doi:10.1029/2006JE002849.

Parker, T. J., M. P. Golombek, and M. W. Powell (2010), Geomorphic/geologic mapping, localization, and traverse planning at the Opportunity landing site, *Lunar Planet. Sci.*, *XLI*, Abstract 2638.

Rice, M. S., J. F. Bell III, E. A. Cloutis, J. J. Wray, K. E. Herkenhoff, R. Sullivan, and J. R. Johnson (2011), Temporal observations of bright soil exposures at Gusev crater, Mars, *J. Geophys. Res.*, doi:10.1029/2010JE003683, in press.

Schröder, C., et al. (2008), Meteorites on Mars observed with the Mars Exploration Rovers, *J. Geophys. Res.*, *113*, E06S22, doi:10.1029/2007JE002990.

Schröder, C., et al. (2010), Properties and distribution of paired stony meteorite candidate rocks at Meridiani Planum, Mars, *J. Geophys. Res.*, *115*, E00F09, doi:10.1029/2010JE003616.

Soderblom, L. A., et al. (2004), Soils of Eagle crater and Meridiani Planum at the Opportunity rover landing site, *Science*, *306*, 1723–1726, doi:10.1126/science.1105127.

Sprague, A. L., W. V. Boynton, K. E. Kerry, D. M. Janes, N. J. Kelly, M. K. Crombie, S. M. Melli, J. R. Murphy, R. C. Reedy, and A. E. Metzger (2007), Mars' atmospheric argon: Tracer for understanding Martian atmospheric circulation and dynamics, *J. Geophys. Res.*, *112*, E03S02, doi:10.1029/2005JE002597.

Squyres, S., and A. H. Knoll (2005), Outcrop geology at Meridiani Planum: Introduction, *Earth Planet. Sci. Lett.*, *240*, 1–10, doi:10.1016/j.epsl.2005.09.038.

Squyres, S. W., et al. (2003), Athena Mars rover science investigation, *J. Geophys. Res.*, *108*(E12), 8062, doi:10.1029/2003JE002121.

Squyres, S. W., et al. (2004), The Opportunity Rover's Athena science investigation at Meridiani Planum, Mars, *Science*, *306*, 1698–1703, doi:10.1126/science.1106171.

Squyres, S. W., et al. (2006), Overview of the Opportunity Mars Exploration Rover Mission to Meridiani Planum: Eagle crater to Purgatory ripple, *J. Geophys. Res.*, *111*, E12S12, doi:10.1029/2006JE002771.

Squyres, S. W., et al. (2008), Detection of silica-rich deposits on Mars, *Science*, *320*, 1063–1067, doi:10.1126/science.1155429.

Squyres, S. W., et al. (2009), Exploration of Victoria crater by the Mars Rover Opportunity, *Science*, *324*, 1058–1061, doi:10.1126/science.1170355.

Sullivan, R. J., et al. (2005), Aeolian processes at the Mars Exploration Rover Meridiani Planum landing site, *Nature*, *436*(7047), 58–61, doi:10.1038/nature03641.

Sullivan, R. J., et al. (2010), Cohesions, friction angles, and other physical properties of Martian regolith from MER wheel trenches and wheel scuffs, *J. Geophys. Res.*, doi:10.1029/2010JE003625, in press.

Tillman, J. E., N. C. Johnson, P. Guttorp, and D. B. Percival (1993), The Martian annual atmospheric pressure cycle: Years without great dust storms, *J. Geophys. Res.*, *98*, 10,963–10,971, doi:10.1029/93JE01084.

Ward, W. R., and D. J. Rudy (1991), Resonant obliquity of Mars?, *Icarus*, *94*, 160–164, doi:10.1016/0019-1035(91)90146-K.

Weitz, C. M., et al. (2010), Visible and near-infrared multispectral analysis of geochemically measured rock fragments at the Opportunity landing site in Meridiani Planum, *J. Geophys. Res.*, *115*, E00F10, doi:10.1029/2010JE003660.

Wolff, M. J., P. B. James, T. R. Clancy, and S. W. Lee (1999), Hubble Space Telescope observations of the Martian aphelion cloud belt prior to the Pathfinder mission: Seasonal and interannual variations, *J. Geophys. Res.*, *104*, 9027–9041, doi:10.1029/98JE01967.

Wong, J. (2003), *Theory of Ground Vehicles*, 2nd ed., John Wiley, New York.

Wray, J. J., E. Z. Noe Dobrea, R. E. Arvidson, S. M. Wiseman, S. W. Squyres, A. S. McEwen, J. F. Mustard, and S. L. Murchie (2009), Phyllosilicates and sulfates at Endeavour crater, Meridiani Planum, Mars, *Geophys. Res. Lett.*, *36*, L21201, doi:10.1029/2009GL040734.

Zipfel, J., et al. (2011), Bounce Rock: A shergottite-like basalt encountered at Meridiani Planum, Mars, *Meteorit. Planet. Sci.*, in press.

R. E. Arvidson, E. A. Guinness, and B. L. Jolliff, Department of Earth and Planetary Sciences, Washington University, St. Louis, MO 63130, USA. (arvidson@rsmail.wustl.edu)

J. W. Ashley, School of Earth and Space Exploration, Mars Space Flight Facility, Arizona State University, Tempe, AZ 85287, USA.

J. F. Bell III, M. S. Rice, S. W. Squyres, and R. J. Sullivan, Department of Astronomy, Cornell University, Ithaca, NY 14853, USA.

M. Chojnacki, Planetary Geosciences Institute, Department of Earth and Planetary Sciences, University of Tennessee, Knoxville, TN 37996, USA.

J. Cohen, Honeybee Robotics Spacecraft Mechanisms Corporation, 460 W. 34th St., New York, NY 10001, USA.

T. E. Economou, Laboratory for Astrophysics and Space Research, Enrico Fermi Institute, University of Chicago, Chicago, IL 60637, USA.

W. H. Farrand and M. J. Wolff, Space Science Institute, 4750 Walnut St., Ste. 205, Boulder, CO 80301, USA.

R. Fergason, P. Geissler, K. E. Herkenhoff, J. R. Johnson, and L. A. Soderblom, U.S. Geological Survey, 2255 N. Gemini Dr., Flagstaff, AZ 86001, USA.

I. Fleischer and G. Klingelhöfer, Institut für Anorganische und Analytische Chemie, Johannes Gutenberg-Universität, D-55099 Mainz, Germany.

R. Gellert, Department of Physics, University of Guelph, Guelph, ON N1G 2W1, Canada.

M. P. Golombek, J. A. Herman, and T. J. Parker, Jet Propulsion Laboratory, California Institute of Technology, 4800 Oak Grove Dr., Pasadena, CA 91109, USA.

J. P. Grotzinger, Division of Geological and Planetary Sciences, California Institute of Technology, Pasadena, CA 91125, USA.

R. M. Haberle, NASA Ames Research Center, Moffett Field, CA 94035, USA.

K. D. Iagnemma, Department of Mechanical Engineering, Massachusetts Institute of Technology, Cambridge, MA 02139, USA.

A. H. Knoll, Department of Organismic and Evolutionary Biology, Harvard University, Cambridge, MA 02138, USA.

A. T. Knudson, Planetary Science Institute, 1700 East Fort Lowell, Ste. 106, Tucson, AZ 85719, USA.

R. Li, Department of Civil and Environmental Engineering and Geodetic Science, Ohio State University, Columbus, OH 43210, USA.

S. M. McLennan, Department of Geosciences, State University of New York at Stony Brook, Stony Brook, NY 11794, USA.

D. W. Mittlefehldt and R. V. Morris, NASA Johnson Space Center, Houston, TX 77058, USA.

C. Schröder, Center for Applied Geoscience, Eberhard Karls University of Tübingen, Sigwartstr. 10, D-72076 Tübingen, Germany.